File 7143

PB 176 137

ANALYSIS OF OPTIMUM AND PREVIEW CONTROL OF ACTIVE VEHICLE SUSPENSIONS

E. K. Bender

I. L. Paul

Prepared for the U.S. Department of Transportation
under Contract C-85-65

Department of Mechanical Engineering
Engineering Projects Laboratory
Massachusetts Institute of Technology
Cambridge, Massachusetts 02139

September 1, 1967

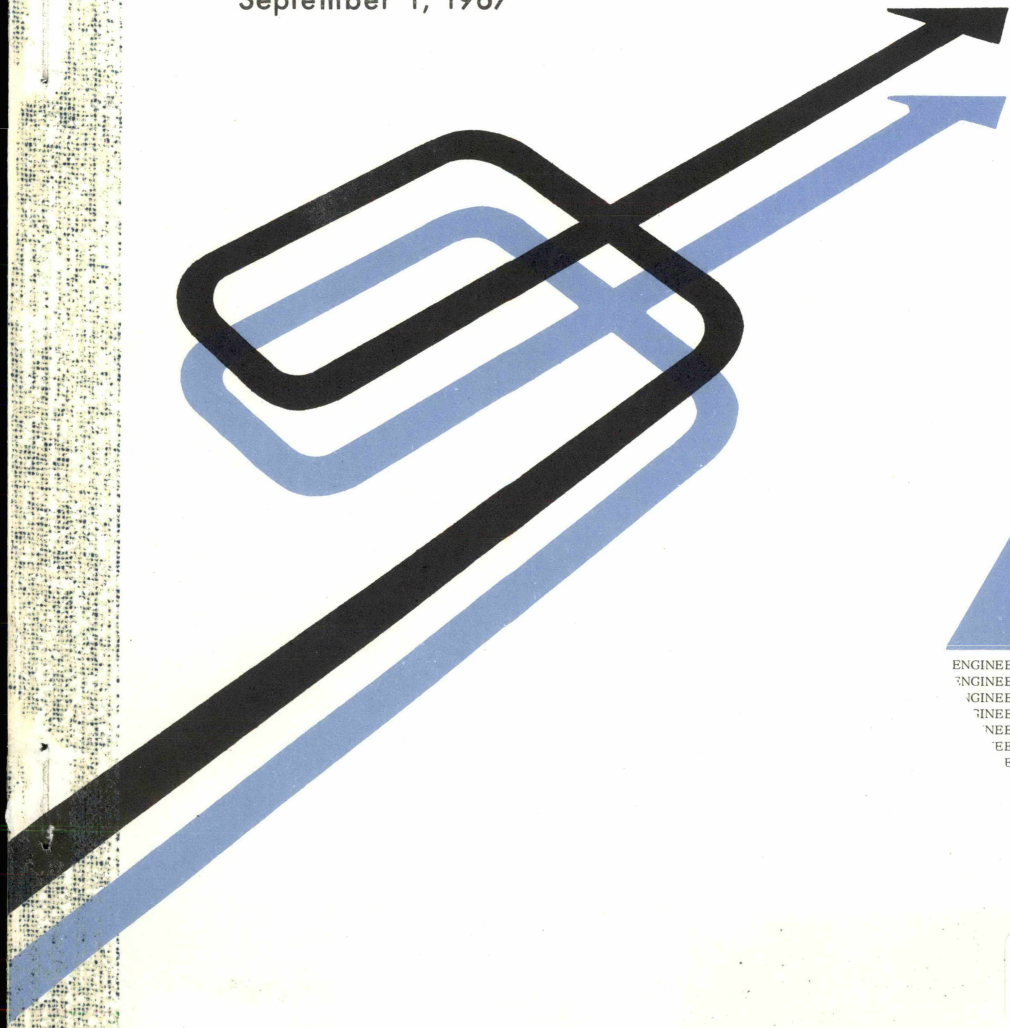

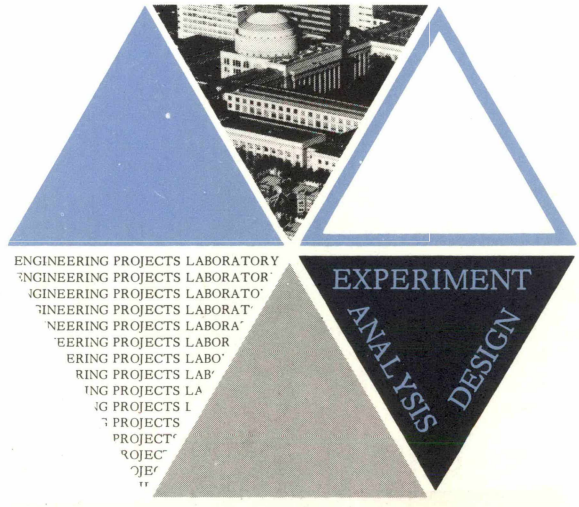

03 - Rail Vehicles &
Components

ANALYSIS OF OPTIMUM AND PREVIEW CONTROL OF ACTIVE VEHICLE SUSPENSIONS

by

ERICH K. BENDER
IGOR L. PAUL

REPORT DSR-76109-6

prepared for the

UNITED STATES DEPARTMENT OF TRANSPORTATION

Washington, D.C.

Under Contract C-85-65

Clearinghouse No. PB 176 137

by the

ENGINEERING PROJECTS LABORATORY
DEPARTMENT OF MECHANICAL ENGINEERING
MASSACHUSETTS INSTITUTE OF TECHNOLOGY
CAMBRIDGE, MASSACHUSETTS

September 1, 1967

ABSTRACT

The analysis leading to the optimum transfer function for an active suspension excited by a random guideway input is briefly reviewed and a design chart is presented. A parameter sensitivity study of the stability is performed and shows excellent system stability. The wheel-guideway contact problem is considered and a design chart is developed to check wheel-guideway relative displacement (wheel hop) for active suspensions. The equations for the rms force required to prevent wheel hop are derived and a design chart showing the minimum rms vehicle acceleration which can be obtained while applying this force is presented. The improved vibration isolation characteristics of active suspensions using preview control are investigated for infinite and finite preview distances. It is found that for a simple model infinite preview can reduce the rms vehicle acceleration by a factor of 16 and that a preview time of .4-.5 seconds is sufficient to provide almost the same improvement as infinite preview. It is concluded that active suspension development for vehicle heave, roll and pitch control, particularly for use with preview control, is warranted.

ACKNOWLEDGEMENT

This work was supported by the U.S. Department of Transportation under Contract C-85-65 and sponsored by the Division of Sponsored Research of M.I.T.

TABLE OF CONTENTS

NOMENCLATURE

a	$k_s/(k_v + k_s)$
A	Roadway spectral density amplitude
B	Coefficient (Appendix A)
c	Damping coefficient
C	Coefficient (Appendix A)
D	Coefficient (Appendix A)
E	Coefficient (Appendix A)
f_s	Sprung mass natural frequency $(\omega_s/2\pi)$
f_u	Unsprung mass natural frequency $(\omega_u/2\pi)$
F	Loading variation, Force
F_s	Suspension Force
$\bar{F}$	$F/8\pi^2\alpha M\sqrt{AVf_u^3}$
g	Gravitational constant
h	Suspension clearance space
H	Transfer function
I	Coefficient (Appendix A)
j	$\sqrt{-1}$
k	Spring rate
k_{01}	Unsprung mass spring rate
k_{12}	Sprung mass spring rate
k_s	Gain of preview controller
k_v	Preview suspension spring rate
K	Feedback gain
L	Preview distance
m	Mass of unsprung mass
M	Mass of sprung mass
n	Constant
P	Penalty function
r	Mass ratio m/M
s	Laplace operator
t	Time
T	Preview time
V	Velocity
W	Synthesized suspension transfer function
W_p	Preview synthesized suspension transfer function
W_w	Synthesized transfer function for minimum rms suspension force
x,X	Roadway elevation; constant
x_s	Roadway elevation at preview sensor
x_v	Roadway elevation at vehicle
y,Y	Sprung mass position; constant
y_s	Response of y to a step in x
z,Z	Unsprung mass position
α	Clearance factor
β	$\rho\omega_u^2$
γ	ω_s/ω_u
$\gamma(t)$	Inverse transform of $\Gamma(s)/\bar{\Delta}(s)$

Γ Synthesizing function

δ z-y

δ_o Static unsprung mass deflection due to vehicle weight

δ_p $x_v - y$

δ_w $z - x$

Δ Synthesizing function

ϵ Small quantity

ζ Damping ratio $c/2\sqrt{k_{12}M}$

ρ Lagrange multiplier or weighting factor

τ $\sqrt{2}\ \rho^{1/4}$

ϕ s/ω_u; s/ω_n in Section V

Φ Power spectral density

ψ $\rho^{1/4}s$

ω Frequency

ω_o Spectrum level-off frequency

ω_n Preview suspension natural frequency $\sqrt{(k_v + k_s)/M}$

ω_s Sprung mass natural frequency $\sqrt{k_{12}/M}$

ω_u Unsprung mass natural frequency $\sqrt{k_{01}/m}$

Ω Wave number (rad./ft.)

LIST OF FIGURES

I. INTRODUCTION

The present report represents an extension of the work reported in References 1 & 2. The procedure and results of that work are very briefly reviewed below to provide background and easy reference for the current analyses.

It has been found [1,2]* that the profile spectrum of representative guideways (runways, highways, etc.) can be conveniently represented by an equation of the form

$$\phi_{xx}(\Omega) = A/\Omega^2 \quad \text{or} \quad \phi_t(\omega) = \frac{AV}{\omega^2} = \frac{AV}{s^2} \tag{1}$$

(nomenclature on page iv). This guideway input acts on a vehicle suspension as shown in Figure 1, where the excursion of the suspension is limited by practical considerations. Sufficient clearance must be provided to allow for load variations as well as dynamic excursions of the unsprung mass as shown in Figure 2. Since we are working with random inputs bottoming of the suspension will occur occasionally (unless prevented by non-linear characteristics near the excursion limits) but can be made infrequent by allowing clearance space needed for dynamic excursions equal to several times (by a factor of α) the rms relative dynamic displacement. Thus

$$h/2 - F/2k = \alpha\delta_{rms} \tag{2}$$

Since there are indications that the roadway elevation distribution is Gaussian, the parameter α should be about 3 to keep the sprung mass from bottoming at least 99.9% of the time.

---

* [ ] indicate references at end of report

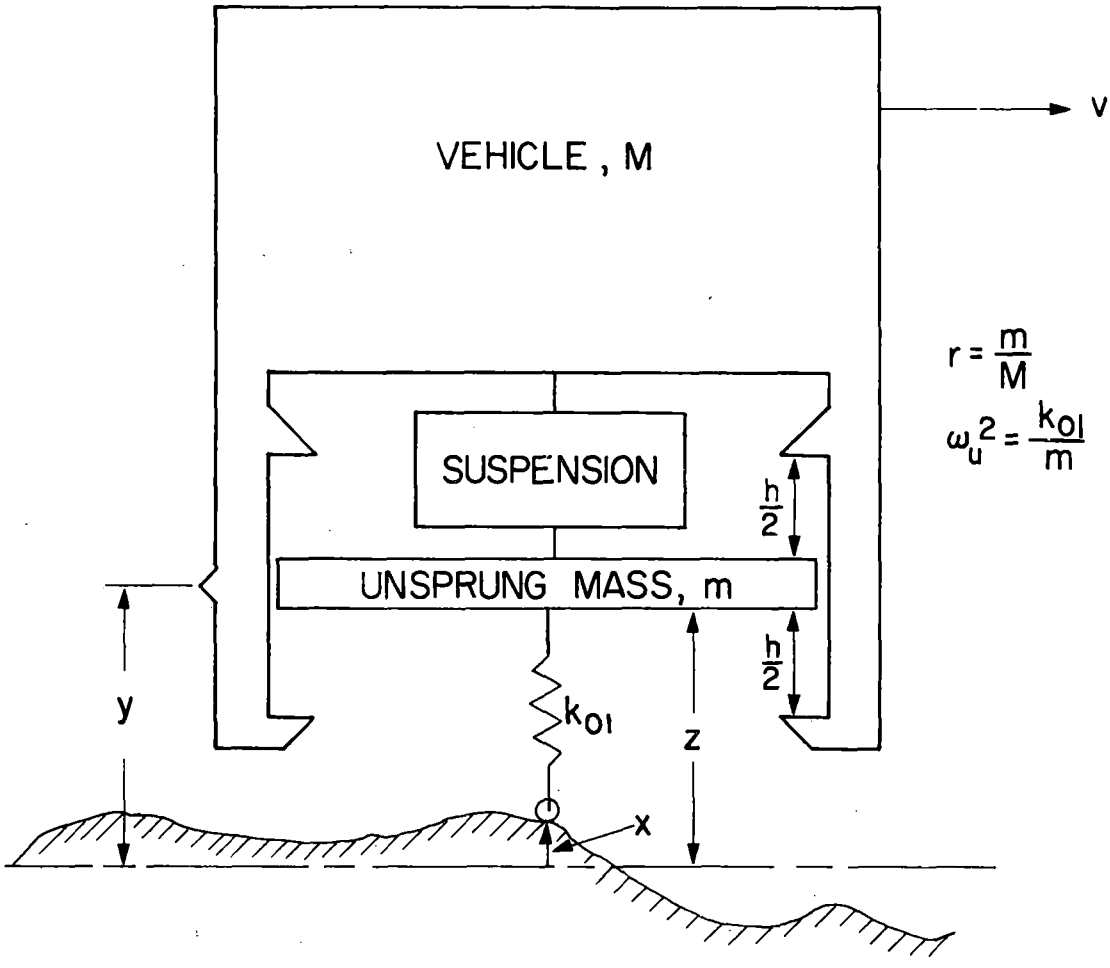

Figure 1. Vehicle - Roadway Configuration

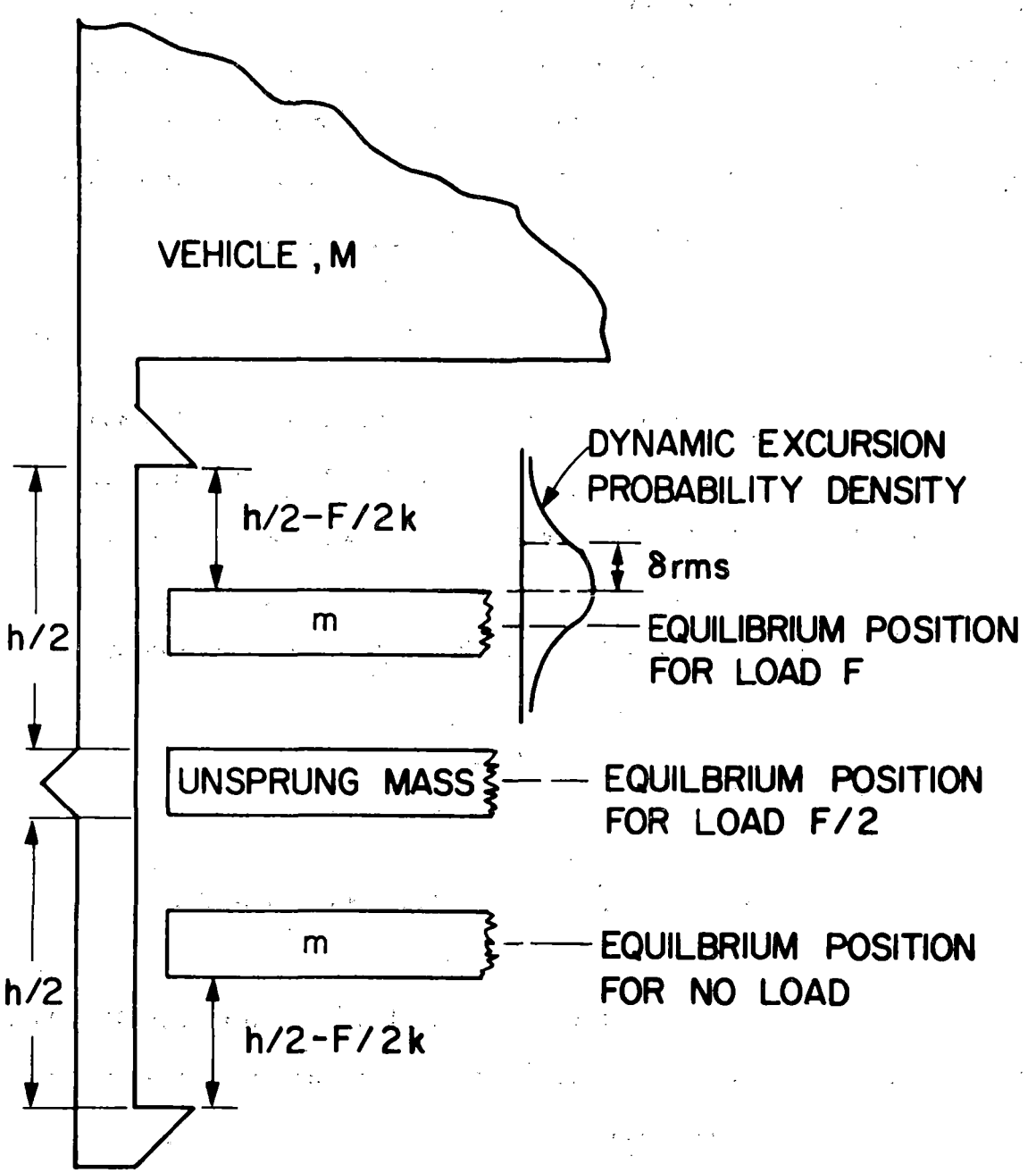

Figure 2. Suspension Deflection Quantities

The clearance required to provide certain vibration isolation characteristics or, conversely, the vibration isolation which can be achieved with a given suspension excursion clearance is thus of prime importance. To optimize the vibration-clearance trade-off, a penalty or cost function, P, is formed which is a linear combination of the rms acceleration, $\ddot{y}_{rms}$, and the clearance space h

$$P = \rho\ddot{y}_{rms} + h = \rho\ddot{y}_{rms} + 2\alpha\delta_{rms} + F/k \tag{3}$$

The parameters of a given suspension transfer function and the transfer function for an unknown suspension which will minimize this penalty function were then derived using variational calculus (ala Wiener filter theory).

The optimum transfer function which minimizes the penalty function was found to be

$$W(\phi) = \frac{\omega_u^2\phi^2[(B+1)\phi^2 + C\phi + 1]}{\sqrt{\beta}\,\phi^4 + 2\sqrt{\beta}\,D\phi^3 + \sqrt{\beta}E\phi^2 + 2\sqrt{\beta}\,I\phi + 1} \tag{4}$$

where the parameters B, C, D and E are defined in Appendix A.

The expression for the rms acceleration $\ddot{y}_{rms}$, non-dimensionalized by the roadway roughness A, vehicle speed V, and unsprung mass natural frequency in Hz, f_u, was then found to be

$$\frac{\ddot{y}_{rms}}{4\pi^2\sqrt{AVf_u^3}} = \left[\frac{1}{2\pi j}\int_{-j\infty}^{j\infty}\frac{W(\phi)}{\phi}\cdot\frac{W(-\phi)}{-\phi}\cdot d\phi\right]^{1/2} \tag{5}$$

or with the help of tabulated algebraic expressions for the above integral, the acceleration becomes

$$\frac{\ddot{y}_{rms}}{4\pi^2\sqrt{AVf_u^3}} = \left[\frac{(B+1)^2(2\sqrt{\beta}EI - \sqrt{2}\,D) + (C^2 - 2B - 2)2\sqrt{\beta}\,I + 2\sqrt{\beta}D}{8\beta\,(\sqrt{\beta}DEI - D^2 - \sqrt{\beta}I^2)}\right]^{1/2} \tag{6}$$

where B, C, D, E, and I are evaluated in Appendix A. Similarly, the clearance space $h = 2\alpha\delta_{rms}$ is given by

$$\frac{h}{2\alpha}\sqrt{\frac{f_u}{AV}} = \left[\frac{\sqrt{\beta} - (B+1)(1+1/r)^2\,2D + [2\sqrt{\beta}\,D - C(1+1/r)]^2 2\sqrt{\beta}(DE - I)}{8(\beta\,DEI - \sqrt{\beta}D^2 - \beta I^2)}\right]^{1/2} \tag{7}$$

The vibration-clearance space trade-off for the optimum synthesized suspension corresponding to a given mass ratio, r, is then found as follows:

a) Choose a value of β, compute B, C, D, E, and I (see Appendix A) and then find the rms acceleration and the clearance space from the above two equations; b) Increment β and repeat the whole procedure. The points on a vibration-clearance plot thus found define a curve which is a lower bound to the performance of suspensions which are linear, do not use preview information, and apply equal forces to the unsprung and sprung masses. This optimum trade-off curve is shown for $r = 0.1$ in a design chart (Figure 3) along with curves for passive, fixed configuration systems.

This design chart shows the sprung mass rms acceleration which can be obtained with a given clearance space using passive

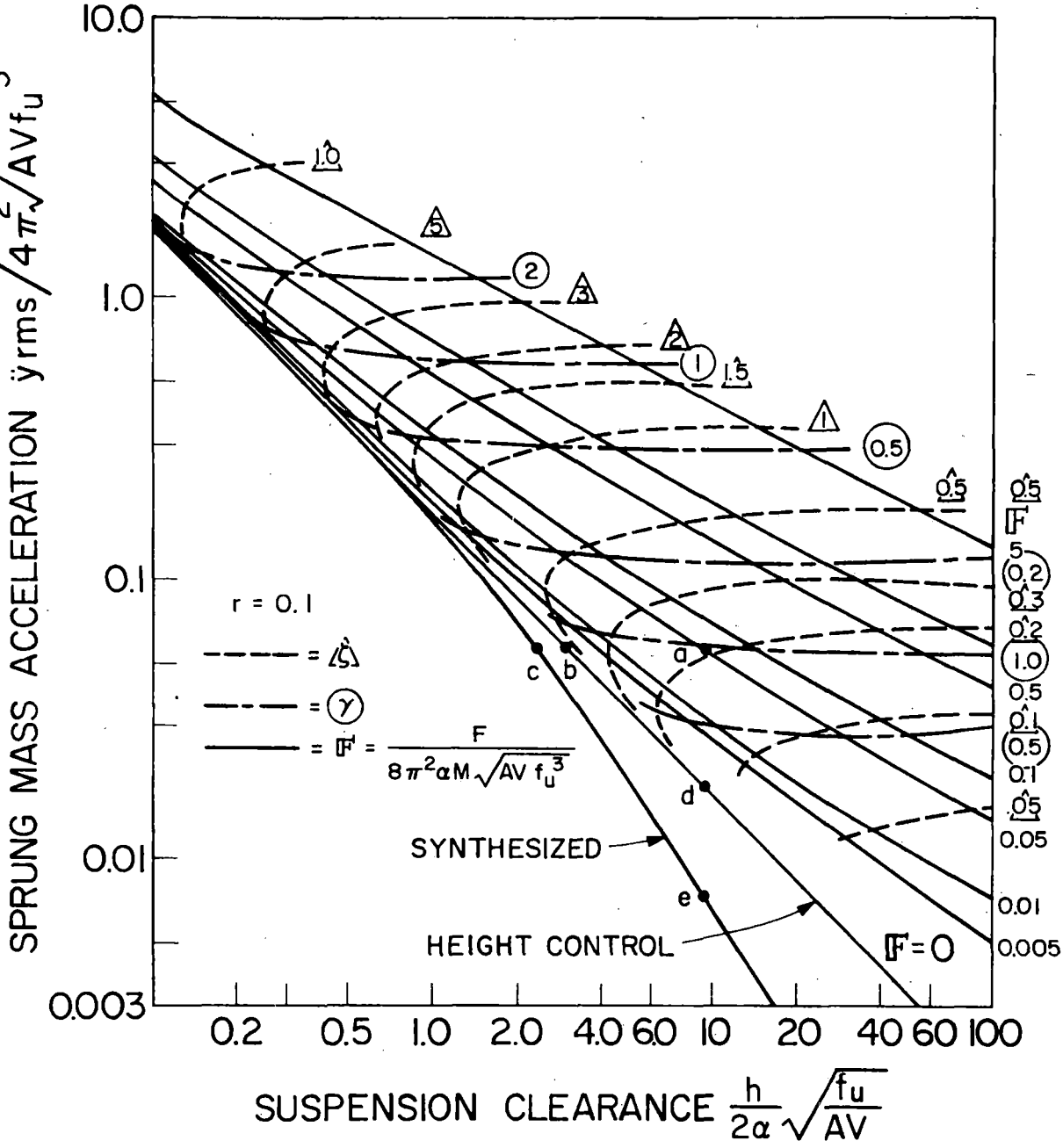

Figure 3. Acceleration - Suspension Clearance Design Chart

systems, automatic height control and synthesized active suspensions without preview information.

These curves assume that the wheel is restrained to follow the guideway profile (no wheel hop, positive and negative forces between guideway and wheel are permissible). The present report extends the analysis to include the wheel-guideway contact problem and additional design charts are generated to be used in conjunction with Figure 3 to check for wheel hop.

The analysis is also extended to investigate the beneficial effects of finite and infinite preview control in which case the active suspension can anticipate guideway disturbance inputs.

II. OPTIMUM SYNTHESIZED SUSPENSION

A. Mechanization of Synthesized Suspension

Various control system configurations have transfer functions which can be made to match the transfer function of Equation (4) which has been mathematically synthesized. The procedure followed here is to consider variables which are easily measured and filtered to generate a control force command signal (see Figure 4). Accelerometers may be used to measure unsprung and sprung mass accelerations. Each signal may be filtered by a function of the form $(K_a + K_v/s)$ and then summed to form a command signal. Amplifier and servomechanism dynamics need to be considered in a specific design study but are neglected in this preliminary treatment. In addition, forces proportional to unsprung mass-sprung mass relative displacement and velocity may be generated either passively by springs and shock absorbers or actively by a variety of transducers, amplifiers, and actuators. Thus the control force is assumed to be of the form

$$F_s = (cs + k_{12})(z - y) - K_{sa}s^2y - K_{sv}sy + K_{ua}s^2z + K_{uv}sz \qquad (8)$$

where the nomenclature is defined in Figure 4. The transfer function relating sprung mass acceleration to roadway elevation becomes

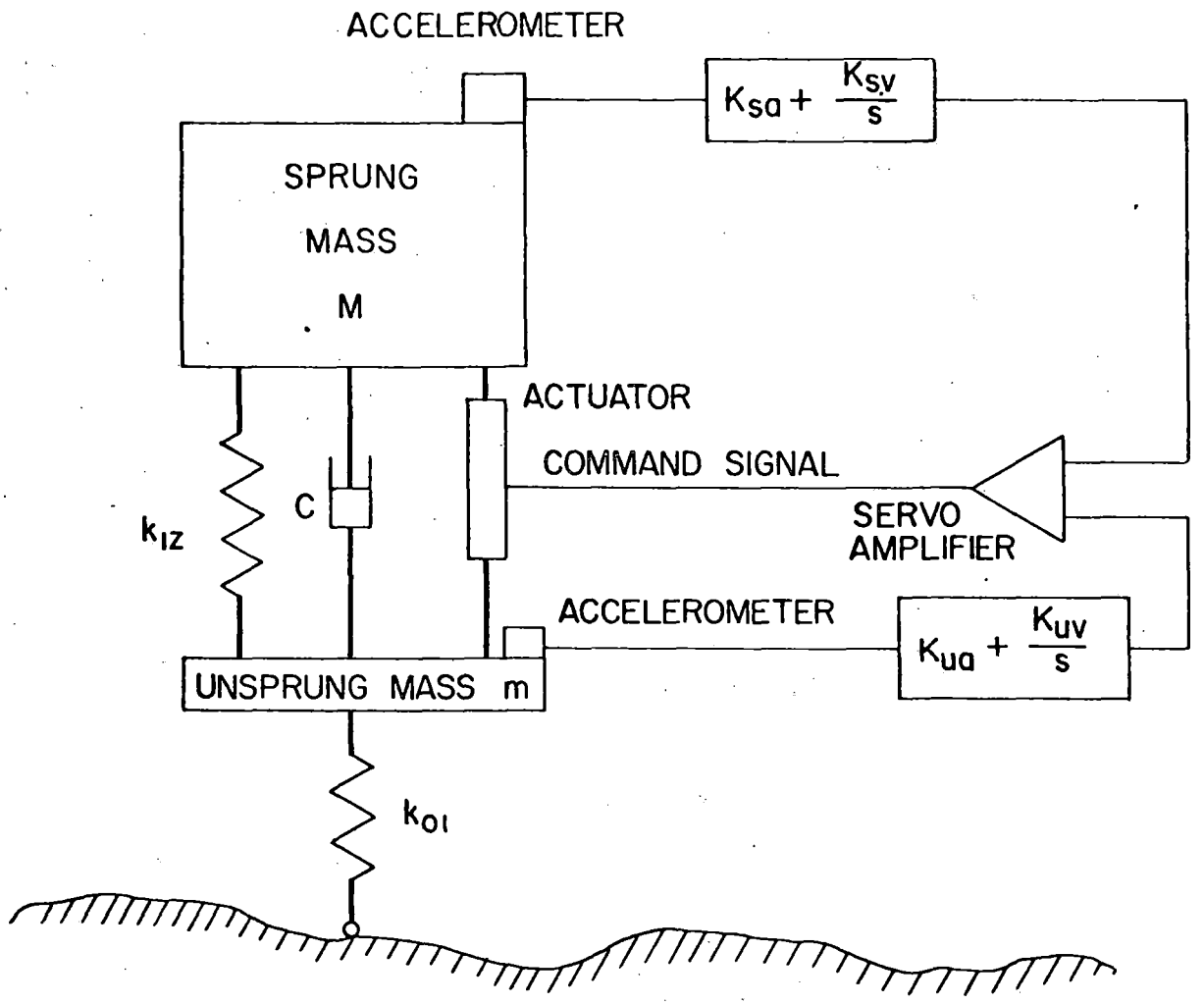

Figure 4. Schematic Diagram of Active Suspension

$$\frac{\ddot{y}(\phi)}{x(\phi)} = \frac{\omega_u^2 \phi^2 [\frac{rK_{ua}}{\gamma^2 m} \phi^2 + (\frac{2\zeta}{\gamma} + \frac{r K_{uv}}{\gamma^2 m \omega_u})\phi + 1]}{\gamma^{-2}(1 + \frac{K_{sa}}{M} + \frac{K_{ua}}{m})\phi^4 + [\frac{2\zeta(1 + 1/r)}{\gamma} + \frac{K_{sv}}{\gamma^2 M \omega_u} + \frac{K_{uv}}{\gamma^2 m \omega_u}]\phi^3}$$

$$+ (\gamma^{-2} + \frac{K_{sa}}{\gamma^2 M} + 1 + 1/r)\phi^2 + (\frac{2\zeta}{\gamma} + \frac{K_{sv}}{\gamma^2 M \omega_u})\phi + 1 \qquad (9)$$

$$\text{where } \gamma^2 = k_{01}M/k_{12}m; \quad \zeta = c/2\sqrt{k_{12}M} .$$

The block diagram for the general active suspension system described by Equation (9) is shown in Figure 5.

The active suspension system can be made optimum by equating coefficients of like power of ϕ in the numerators and in the denominators of Equations (4) and (9). There is some redundancy of parameters. For example, K_{uv} can be zero and γ or K_{sa} chosen arbitrarily. If γ is arbitrary, the spring stiffness, k, may be made as large as hardware limitations permit in order to minimize the effects of externally applied vehicle forces. In order to realize optimum suspension performance, it is essential that the actuator force depends in part on unsprung mass acceleration.

The non-dimensional equations relating the parameters used in the active suspension described by Equation (9) to the coefficients of ρ in the optimum synthesized transfer function are (for $K_{uv} = 0$):

$$\gamma = \left[\frac{1 + K_{sa}/M}{\sqrt{\beta} - B(1 + 1/r)}\right]^{1/2}$$

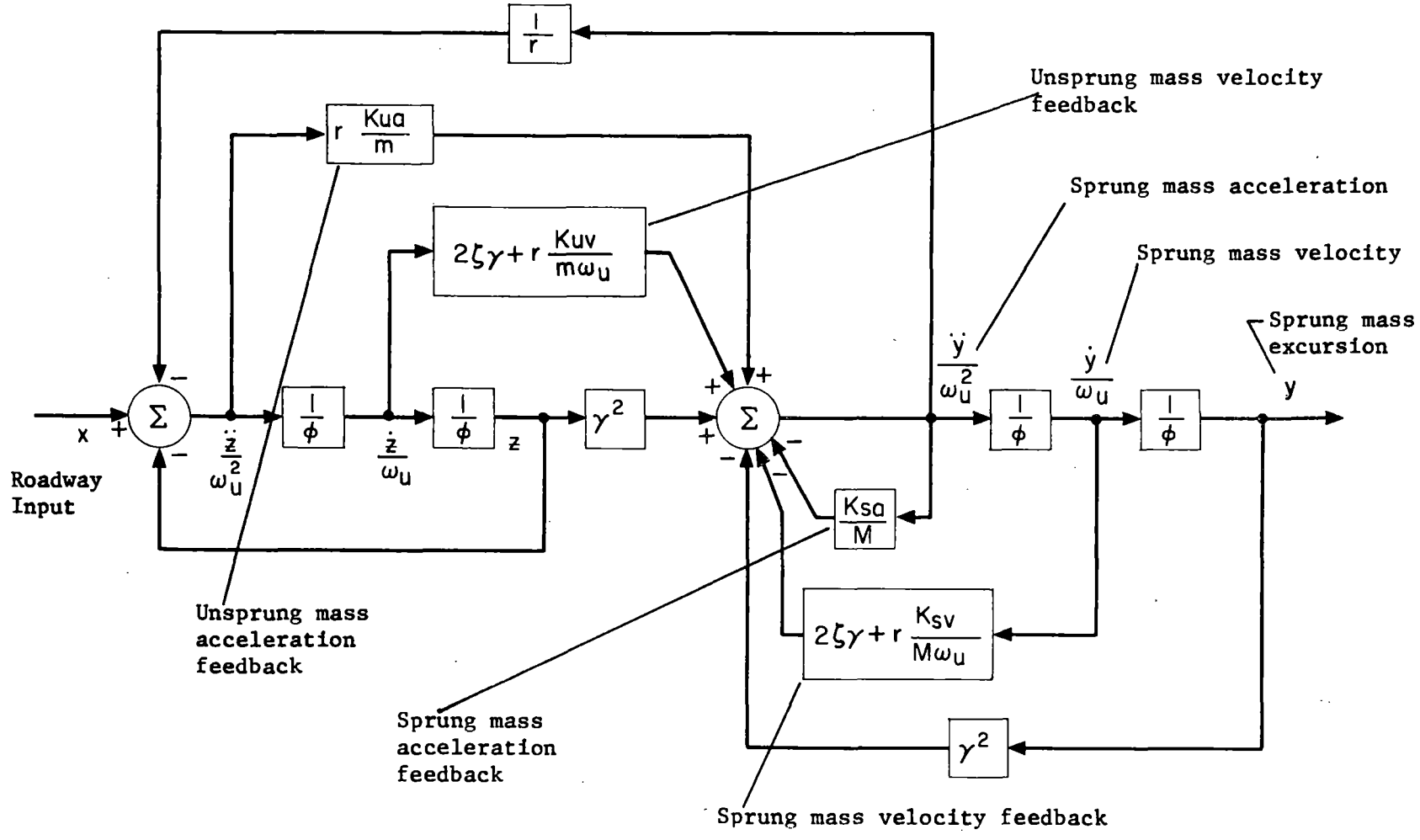

Figure 5. Active Suspension System Block Diagram

$$\frac{K_{ua}}{m} = \gamma^2(B + 1)/r$$

$$\zeta = \frac{1}{2}\gamma C \qquad (10)$$

$$\frac{K_{sv}}{M\omega_u} = 2\sqrt{\beta}\, D\gamma^2$$

Since it is desirable to build as simple a system as possible, one can choose K_{sa} equal to zero to minimize the number of feedback variables. The parameters γ, K_{ua}/m, ζ, and $K_{sv}/M\omega_u$ are computed from the above equations and plotted in Figure 6.

In a rather lengthy theoretical synthesis study such as this, one often wonders if the results (the design chart, Figure 3, and optimum parameter chart, Figure 6) are valid. To confirm the above results, a parameter search optimization was performed. The rms acceleration, $\ddot{y}_{rms}$, and relative displacement, δ_{rms}, were expressed in terms of the system parameters γ, K_{ua}/m, ζ, and $K_{sv}/M\omega_u$ and substituted into the expression for the penalty function P [Equation (3) with F = 0]. P was then minimized for several values of the weighting factor ρ by a hill climbing type of digital computer parameter search program (see Appendix C.). The results of this independent optimization procedure confirm those found by the synthesis method.

B. Sensitivity Analysis

In addition to determining the optimum parameter values

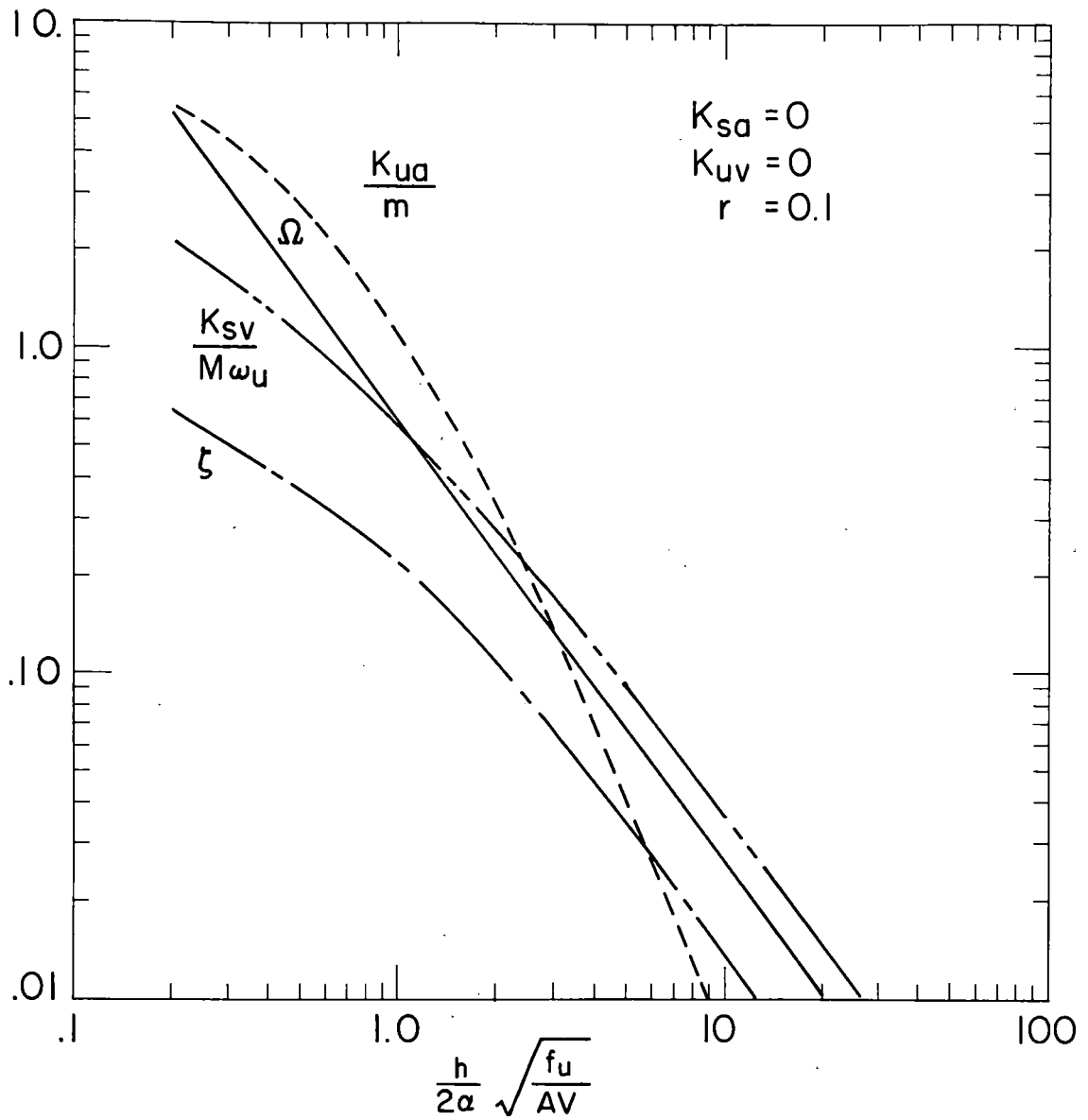

Figure 6. Optimum Active System Parameter Values

from Figure 6, it is desirable to examine the roots of the synthesized system characteristic equation. The roots indicate system resonant frequencies and damping ratios that should be known before any complete system design is undertaken. In practice, it is not generally possible to build a system with the precise parameter values specified by an initial design study. Consequently, one should be aware of the sensitivity of system performance to deviations in values of parameters from the optimum. It is especially important to determine the effects of parameter variations on stability.

Each of the roots of the characteristic equation for the optimum synthesized system depends only on the weighting factor β. One may therefore plot the poles of the optimum transfer function (Equation 9) as a function of β. The root locus shown in Figure 7 was found by computing the coefficients of the synthesized system characteristic equation and extracting the roots with the aid of a digital computer program. It should be emphasized that this root locus is not the conventional type where only one gain is varied. Here all gains are varied according to the above parameter computation scheme. It may be seen that at very low and very large values of β, corresponding to high and low acceleration levels, there will be very lightly damped system poles. These poles might be a problem if they occur at frequencies near other structural resonant frequencies not accounted for in our preliminary investigation. In addition, one might think that a small change in parameter values from the optimum could shift these poles into the right-half plane, making the system unstable.

A sensitivity analysis was performed to determine the

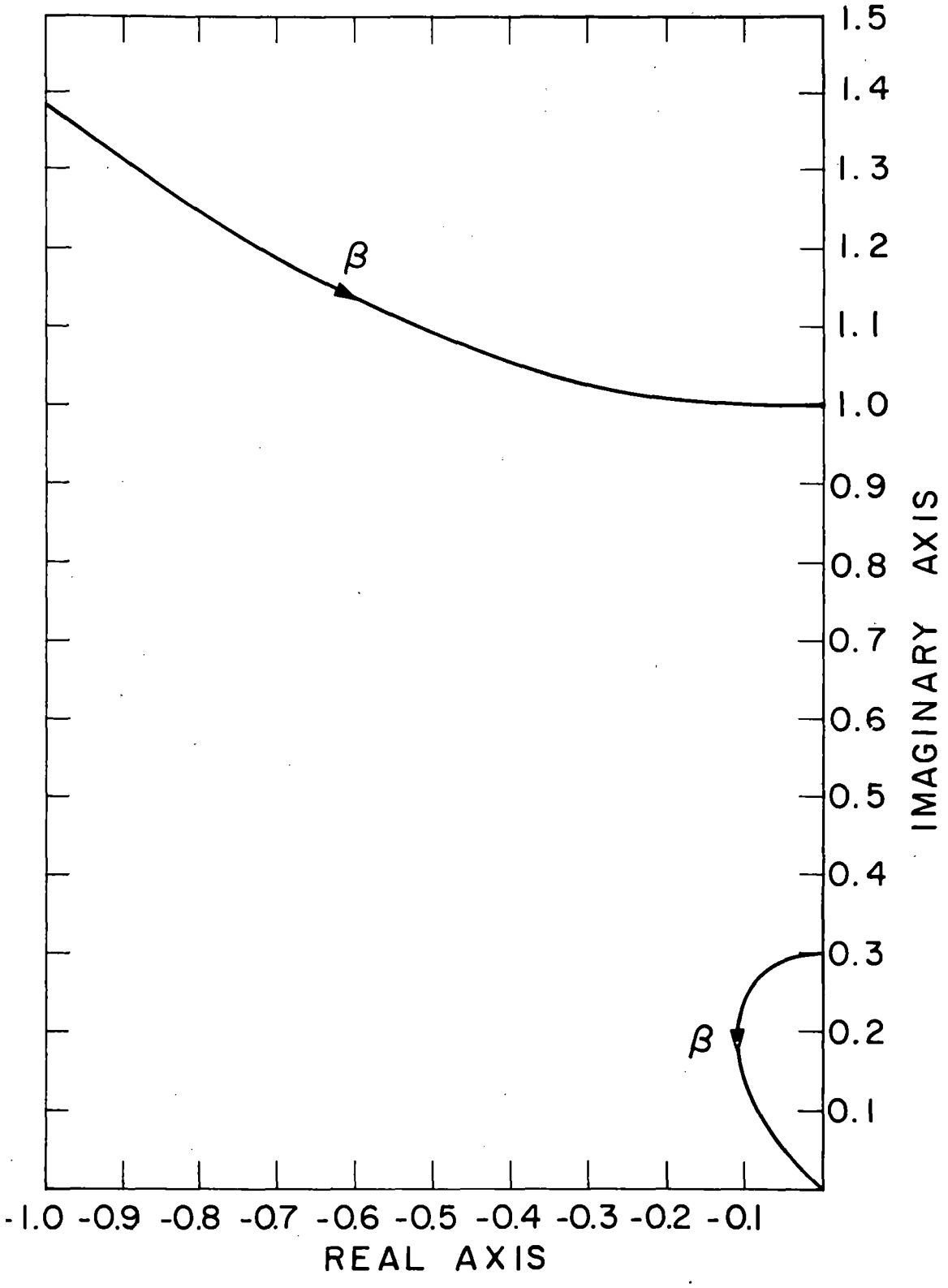

Figure 7. Roots of Optimum Synthesized Transfer Function

percentage by which parameters (the mass ratio, r, and those specified by Figure 6) would have to be varied in order to make the system unstable. First, to find destabilizing directions, each parameter was incremented plus and minus 10% while the other parameters were held fixed at their optimum values. This was done both for large ($\approx 10^6$) and small (≈ 1.0) values of β. Once the destabilizing directions were found by this method the roots of "worst case" combinations were found for several percentage parameter variations. The results were somewhat surprising in two respects. First, the fractional distance a pole shifted toward the right half plane is approximately the same at any of the three points in Figure 7 where the roots approach the imaginary axis. Thus, there does not seem to be any greater tendency for poles near the right half plane to become unstable than for poles further from the imaginary axis. Secondly, it was found that every parameter could be varied as much as 50% in the destabilizing direction without causing instability. One would, therefore, not expect severe stability problems in using the optimum parameters of Figure 6 to mechanize vehicle systems that reasonably fit the model chosen for this investigation (Figure 4).

III. WHEEL-GUIDEWAY INTERACTION

The emphasis, so far, has been on active and passive suspension systems which are optimum only with respect to the vibration-clearance trade-off discussed previously. Whether these optimum systems represent satisfactory designs depends on other criteria not accounted for in the original penalty or cost function. One of the more important of these is the requirement that wheels maintain nearly continuous contact with the guideway if they are not constrained to follow the profile by the guideway, i.e., conventional wheels. The relationships between wheel-guideway dynamics and other dynamic and economic factors of interest such as maneuverability, traction, and wear are not well defined. However, it is certain that each of these qualities will be adversely affected by any appreciable loss of wheel-ground contact. By restricting the rms dynamic deflection $\delta_{w,rms}$ of the wheels with respect to the guideway to $1/\alpha_w$ of the static deflection δ_o of the unsprung mass due to vehicle weight, wheel roadway contact may be maintained for an acceptable proportion of time. For $\alpha_w = 3$, for example, wheels should contact the road for 99.9% of the time since roadway elevation probability density functions tend to be gaussian.

In this section two aspects of wheel-roadway contact will be examined. First, a method and appropriate chart will be developed for determining the degree to which the wheels of suspension systems described by the vibration-clearance design chart (Figure 3) hold the road. Secondly, the minimum rms force required to hold the wheels of a moving vehicle on the road will be determined. Since this force is generally applied to the sprung mass (as contrasted to a

vibration absorber, for example) and since it increases with velocity, one will be able to determine upper speed limits of a vehicle for any given rms sprung mass vibration level.

A. Design Chart Constraint

One may test whether or not optimum suspensions are satisfactory in regard to unsprung mass excursions relative to the guideway by first computing the static deflection of the unsprung mass, δ_o, and then the rms dynamic deflections, $\delta_{w,rms}$ for any particular design. If δ_o is greater than $\delta_{w,rms}$ by a factor of three or more, for example, it can be assumed that a wheeled vehicle would possess adequate wheel-guideway contact. On the other hand, if δ_o is not three or more times larger than $\delta_{w,rms}$, then $\delta_{w,rms}$ should either be included in the penalty function and a new optimization should be performed or the optimum system should be modified to have good, though not optimum, vibration, clearance space, and wheel-guideway characteristics.

The static deflection of the unsprung mass is easily computed as the weight of both sprung and unsprung masses divided by the stiffness k_{01}. Thus

$$\delta_o = \frac{(m + M)g}{k_{01}} \tag{11}$$

where g is the gravitational constant. For a mass ratio m/M of 0.1 the static deflection in feet is

$$\delta_o = 9.0/f_u^2 \tag{12}$$

where f_u is the unsprung mass natural frequency in Hz.

The rms dynamic excursion is found from the transfer function relating guideway elevation to δ_w and the guideway mean square elevation spectral density. The transfer function for δ_w, derived for the general active suspension system (Figure 4), is

$$\frac{\zeta_w}{x}(\phi) = \frac{\phi^2\left(1 + \frac{K_{sa}}{M} + \frac{K_{ua}}{m}\right)\phi^2 + \left[2\zeta\gamma(1 + 1/r) + \frac{K_{sv}}{M\omega_u}\right]\phi + \gamma^2(1 + 1/r)}{\left(1 + \frac{K_{sa}}{M} + \frac{K_{ua}}{m}\right)\phi^4 + \left[2\zeta\gamma(1 + 1/r) + \frac{K_{sv}}{M\omega_u} + \frac{K_{uv}}{m\omega_u}\right]\phi^3}$$

$$+ \left[\gamma^2(1 + 1/r) + 1 + \frac{K_{sa}}{M}\right]\phi^2 + \left(2\zeta\gamma + \frac{K_{sv}}{M\omega_u}\right)\phi + \gamma^2 \qquad (13)$$

From the above and Equation (1) the wheel-guideway rms dynamic excursion is computed for the optimum systems specified by Figure 3. The results are shown in Figure 8 as a function of the non-dimensionalized design clearance.

The shape of the curves in Figure 8 may be explained by physical reasoning. The suspensions corresponding to the left-hand side of Figure 8 are designed for small clearance and are consequently quite stiff. Thus, as clearance space becomes smaller, the sprung and unsprung masses become more nearly locked together as one unit atop the undamped spring represented by k_{01}. This system approaches a single-degree-of-freedom lightly damped oscillator which exhibits considerable relative excursions when excited by a random input. At the right-hand side of Figure 8, $\delta_{w,rms}$ again increases with distance from the central

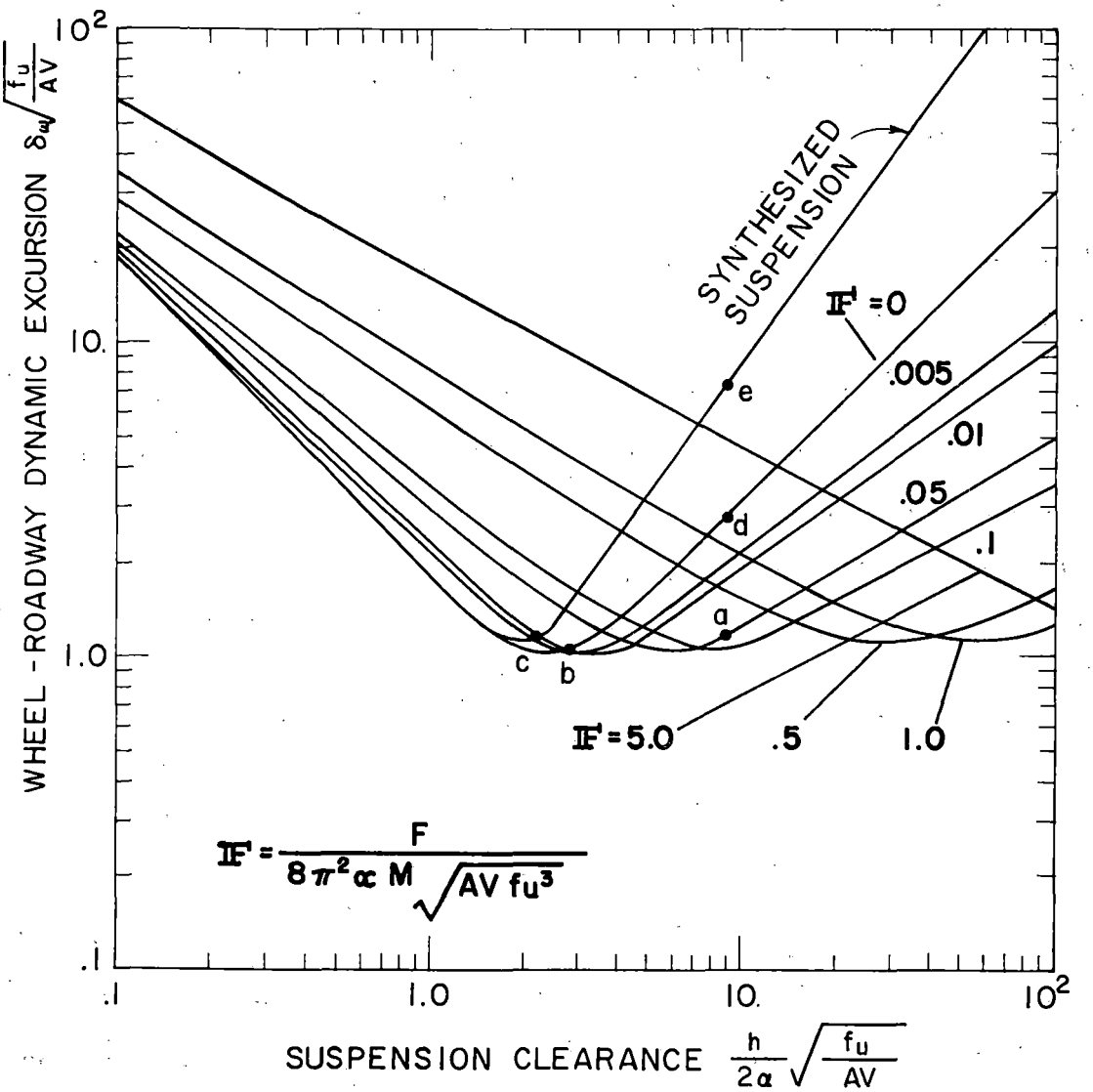

Figure 8. Wheel - Roadway Excursion for Optimum Suspensions Specified by Figure 6

minimum. In this case, however, systems are designed for very low acceleration levels, hence small force transmissibility. As the suspension forces become lower, the unsprung mass becomes increasingly isolated from the sprung mass and behaves like a lightly damped resonant oscillator.

The procedure for testing whether any particular optimum system satisfies the unsprung mass dynamic excursion constraint is now straightforward. First, the static deflection is computed from Equation (11). Then the value of $\delta_{w,rms}\sqrt{f_u/AV}$ (hence $\delta_{w,rms}$), which corresponds to the same trade-off curve and clearance space used in the optimum suspension design chart, is found from Figure 8. Finally $\delta_{w,rms}$ is compared with δ_o to determine if unsprung mass motion is excessive.

B. Minimum RMS Sprung Mass Force

One of the fundamental speed limitations to vehicles using conventional, extremely lightly damped wheels arises from the time varying force required to maintain nearly continuous wheel-road contact. If there were no external forces applied to a wheel, modeled as a single-degree-of-freedom undamped oscillator excited by random roadway elevations, wheel-roadway excursions would be so large that the wheel would bounce a great deal. Since the time varying forces that must be applied to the wheel to keep it on the ground are also applied to the sprung mass (for suspensions that do not incorporate devices such as vibration absorbers), it seems appropriate to attempt to find the minimum rms force, hence rms sprung mass acceleration, required to maintain wheel road contact.

The procedure used here to find the lowest value of rms force needed to provide adequate wheel-guideway contact consists mainly of synthesizing the transfer function relating guideway elevation to suspension force which minimizes the weighted sum of the rms suspension force applied to the wheel plus the rms wheel-guideway dynamic excursion. Thus, there is a trade-off between suspension force and wheel-guideway excursion in much the same way as there is a trade-off between sprung mass acceleration and sprung mass-unsprung mass relative excursion as discussed previously. By letting the rms excursion for this optimum wheel-guideway system be as large as is compatible with road holding requirements ($1/\alpha_w$ of the static displacement) the force is minimal. We will, therefore, find the characteristics of the linear system that can hold the wheels of a vehicle on the road with minimum sprung mass vibration without regard to sprung mass-unsprung mass clearance space.

The equation of motion for an unsprung mass, m, excited by guideway elevation variations x and a suspension force F_s is

$$F_s + k_{01}(x - z) = mz \tag{14}$$

where k_{01} is the wheel stiffness and z is the wheel displacement. Noting that the wheel-guideway relative excursion δ_w is defined by $\delta_w = x - z$ the solution for δ_w in terms of F_s and wheel parameters is

$$\delta_w = \frac{\phi^2}{\phi^2 + 1} x - \frac{Fs/k_{01}}{\phi^2 + 1} \tag{15}$$

By analogy to the block diagram, Figure 5 in Reference 3 with F_s/k_{01},

δ_w and the synthesized wheel-roadway transfer function $W_w(s)$ replacing y, δ, and W(s), respectively, we find that

$$H_1(\phi) = \frac{1}{\phi^2 + 1}$$

$$H_2(\phi) = \frac{\phi^2}{\phi^2 + 1} \tag{16}$$

From Equations (1), (16) and (11) and (12) in Reference 3, the expressions for $\Gamma(\phi)$ and $\Delta(\phi)$ are

$$\Gamma(\phi) = - \frac{2\pi AV/\omega_u^2}{(\phi^2 + 1)^2}$$

$$\Delta(\phi) = - 2\pi AV/\omega_u^2 \left[\frac{\phi^4 + 2\phi^2 + 1 + 1/\rho}{\phi^2(\phi^2 + 1)^2} \right] \tag{17}$$

The numerator of the bracketed term of the above equation may be factored in two stages. First

$$\phi^4 + 2\phi^2 + 1 + 1/\rho = (\phi^2 + 1 + j/\sqrt{\rho})(\phi^2 + 1 - j/\sqrt{\rho}) \tag{18}$$

Then the roots of each of the above bracket terms are found so that $\Delta(\phi)$ is given by

$$\Delta(\phi) = -2\pi\rho AV/\omega_u^2 \frac{(\phi+b+cj)(\phi+b-cj)(\phi-b+cj)(\phi-b-cj)}{\phi^2(\phi^2 + 1)^2} \tag{19}$$

where

$$b = (1 + 1/\rho)^{1/4} \sin \left[\frac{1}{2} \tan^{-1} (1/\sqrt{\rho})\right]$$

$$c = (1 + 1/\rho)^{1/4} \cos \left[\frac{1}{2} \tan^{-1} (1/\sqrt{\rho})\right] \tag{20}$$

Upon factoring $\Delta(\phi)$ into terms, each of which contains roots on opposite sides of the imaginary axis, we have

$$\Delta^{+}(\phi) = \frac{(\phi + b + cj)(\phi + b - cj)}{\phi(\phi^2 + 1)}$$

$$\Delta^{-}(\phi) = -\frac{2\pi AV/\omega_u^{\,2}(\phi - b + cj)(\phi - b - cj)}{\phi(\phi^2 + 1)} \tag{21}$$

Consequently, the expression for $\Gamma(\phi)/\Delta^{-}(\phi)$ is

$$\frac{\Gamma(\phi)}{\Delta^{-}(\phi)} \quad \frac{\phi}{\phi(\phi^2 + 1)(\phi - b + cj)(\phi - b - cj)} \tag{22}$$

If we find that part of the partial fraction expansion of $\Gamma(\phi)/\Delta^{-}(\phi)$, which has only poles in the left-half plane, and divide by $\Delta^{+}(\phi)$, the optimum synthesized transfer function is given by

$$W_w(\phi) = \frac{[(\sqrt{1 + 1/\rho} - 1)\phi + 2b]}{\phi^2 + 2b\phi + \sqrt{1 + 1/\rho}} \tag{23}$$

There are now essentially three steps to find the minimum rms force, $F_{s,rms}$, required to hold the wheels of a moving vehicle on the ground: a) The rms wheel-roadway dynamic excursion $\delta_{w,rms}$ is found; b) by equating $\delta_{w,rms}$ to $1/\alpha_w$ of the static wheel deflection δ_o, an expression containing the weighting factor ρ and various system

parameters is derived. The value of ρ that satisfies this equation corresponds to the minimum rms suspension force; c) the last step is to find the rms force in terms of ρ and solve for $F_{s,rms}$.

From Equations (1), (15), and (23) and noting that $F_s/k_{01} = W_w(s)X(s)$, the expression for $\delta_{w,rms}$ is

$$\delta_{w,rms} = \frac{AV\,(\sqrt{1 + 1/\rho} + 4b^2)}{f_u 4b\,\sqrt{1 + 1/\rho}}^{1/2} \tag{24}$$

By equating α_w times the above equation to the expression for the static wheel deflection [Equation (11)], one obtains

$$\frac{AVf_u^3}{(1 + 1/r)^2 g^2}\ \frac{\alpha_w^2 (2\pi)^4 (\sqrt{1 + 1/\rho} + 4b^2)}{4b\,\sqrt{1 + 1/\rho}} = 1 \tag{25}$$

In a manner completely similar to the derivation of Equation (24), the expression for $F_{s,rms}$ divided by the sprung plus unsprung mass weight $(m + M)g$ is found to be

$$\frac{F_{s,rms}}{(m + M)g} = \frac{AVf_u^3\,(2\pi)^4[(\sqrt{1 + 1/\rho} - 1)^2\sqrt{1 + 1/\rho} + 4b^2]}{(1 + 1/r)^2 g^2\ \ 4b\sqrt{1 + 1/\rho}}^{1/2} \tag{26}$$

We can compute and plot $F_{s,rms}/(m + M)g$ as a function of the parameter AVf_u^3/g^2 for several values of r by using an iterative technique to solve Equation (25) for ρ and then by solving Equation (26) for $F_{s,rms}/(m + M)g$. The results of this analysis for $\alpha_w = 3$, illustrated in Figure 9, show how $F_{s,rms}/(m + M)g$, hence the minimum sprung mass vibration, increases with roadway roughness, vehicle speed, and unsprung mass natural

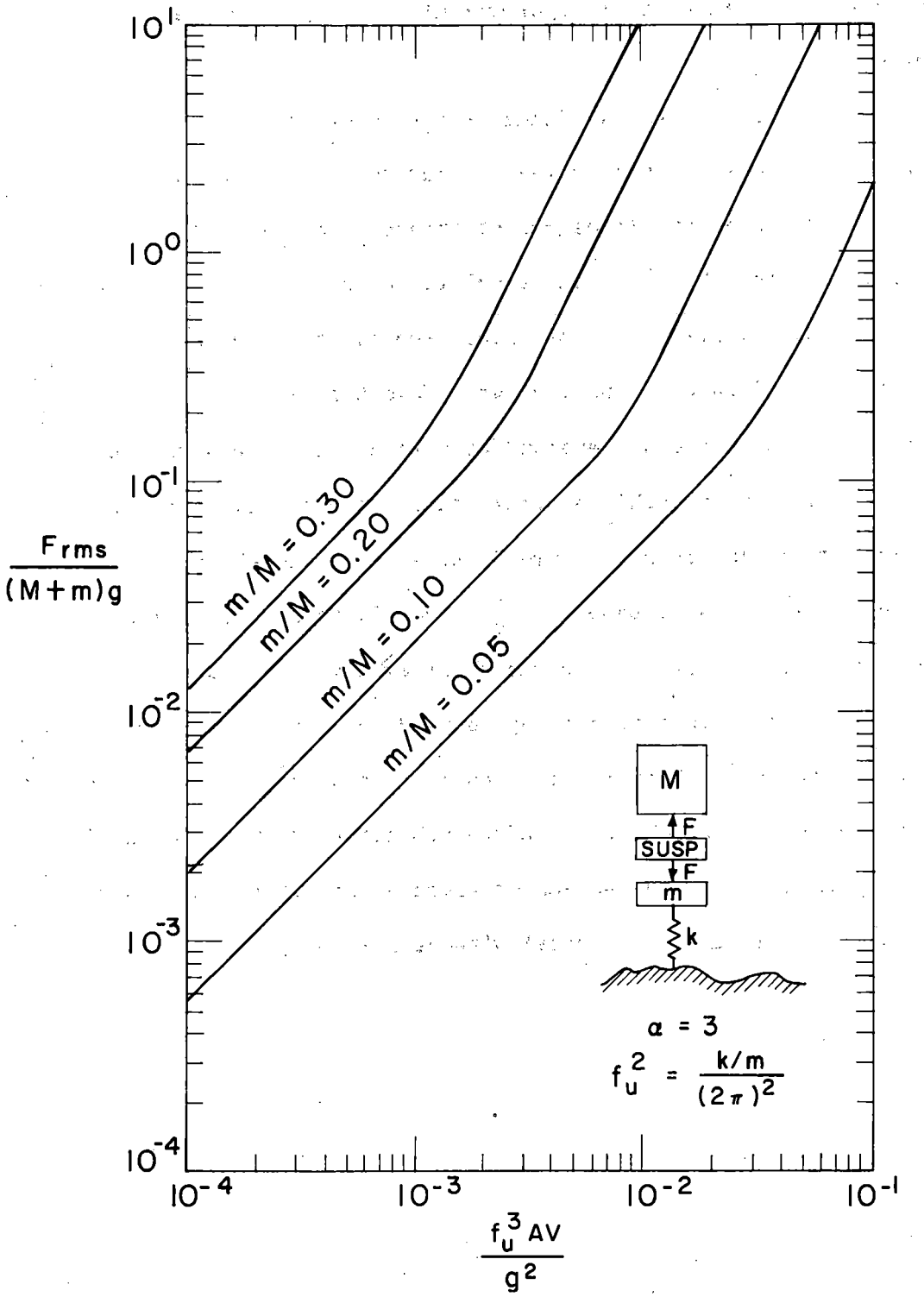

Figure 9. Minimum RMS Force Required to Maintain Wheel - Roadway Contact 99.9% of the Time

frequency. The benefits of light-weight unsprung masses are also apparent.

The curves in Figure 9 represent ultimate speed limitations because of sprung mass vibration only for an unsprung mass modeled as a linear single-degree-of-freedom undamped system and for a linear suspension which applies equal forces to both unsprung and sprung masses. Damping, present in all real wheels, tends to make the results illustrated in Figure 9 conservative. Nevertheless, several steps may be taken to reduce the suspension force required to maintain adequate wheel-road contact if vehicle acceleration is excessive. First, since the rms suspension force is approximately proportional to the cube of the unsprung mass natural frequency, f_u, a considerable sprung mass vibration reduction may be brought about by a moderate decrease in f_u. Secondly, a vibration absorber may be used to reduce the forces applied to the sprung mass. Finally, for vehicles in a tunnel, an overhead suspension system, which might reduce vehicle vibration, could also be used to preload the main suspension thereby permitting large wheel-road excursion (hence small rms force) without loss of wheel-road contact.

IV. OPTIMUM LINEAR PREVIEW CONTROL

The accuracy with which a driver can keep his vehicle at the center of a lane for a given speed depends, among other things, on his visibility of the roadway ahead of the car. Certainly a measure of tracking error (i.e., deviation of the vehicle from the center of the lane) would decrease monotonically with increasing visibility but would reach a finite value even for infinite visibility. Thus, although information regarding the roadway path ahead of a vehicle is significant in controlling an automobile, for long distances such data apparently provide diminishing returns as the preview distance increases.

There is a strong similarity between the function of a human operator to steer a vehicle along a winding road and the function of a suspension to guide a vehicle over the vertical part of a roadway profile. In this section, some of the fundamental limitations and trade-offs pertaining to vehicle suspensions that are capable of utilizing data on the roadway profile ahead of a vehicle are investigated. First, a vehicle model (different from that used previously) and optimum synthesized suspension that does not use preview control will be established. In order to find ultimate performance capabilities, the optimum system transfer function and corresponding accelerations and relative displacements will be found for a system that has infinite roadway preview. Finite preview suspension systems will be studied to determine how vibration and clearance space improvements depend on preview distance. Finally, mechanization of preview suspension systems will be considered.

The vehicle model used for this study is a single-degree-of-freedom rigid mass connected to the roadway by massless suspension elements. Unfortunately, the mathematics in this section are sufficiently lengthy to justify a preliminary study of only the simplest of systems. The model is, however, broadly representative of the fundamental suspension problem of guiding a vehicle over a road with a minimum of vibration and clearance space. Schematically, Figure 10 shows both the vehicle-suspension-guideway configuration and the block diagram relating roadway elevation to vehicle acceleration and to vehicle-roadway clearance space. The roadway elevation at the preview sensor, x_s, is viewed as the input to the synthesized suspension, $W_p(s)$. The vehicle acceleration $\ddot{y}$ is integrated twice to give displacement y which is subtracted from the roadway elevation x_v under the vehicle to give vehicle-roadway relative excursion δ_p. The roadway elevation under a moving vehicle x_v is the same as that at the sensor position but delayed by a time T equal to the distance L of the sensor in front of the vehicle divided by the vehicle velocity V.

A. Zero Preview

The transfer function and vibration clearance trade-off curve for the case of zero preview (L = 0) are useful bases against which to compare similar results for finite and infinite preview suspensions. The expressions for the synthesizing functions $\Gamma(s)$ and $\Delta(s)$ are derived by noting from Figure 12 [Reference 1] and Figure 10b that $H_1(s) = 1/s^2$ and $H_2(s) = 1$.

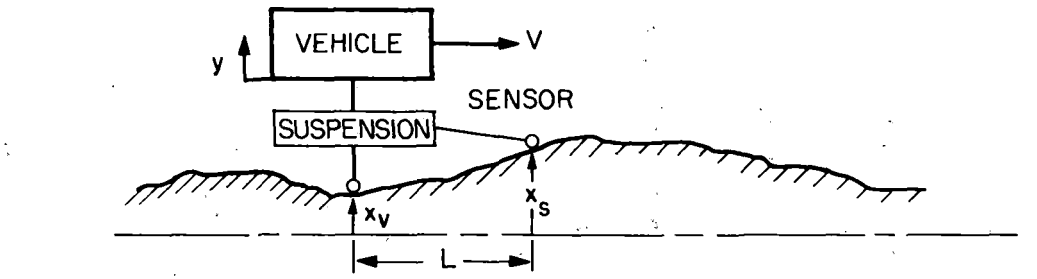

(a)

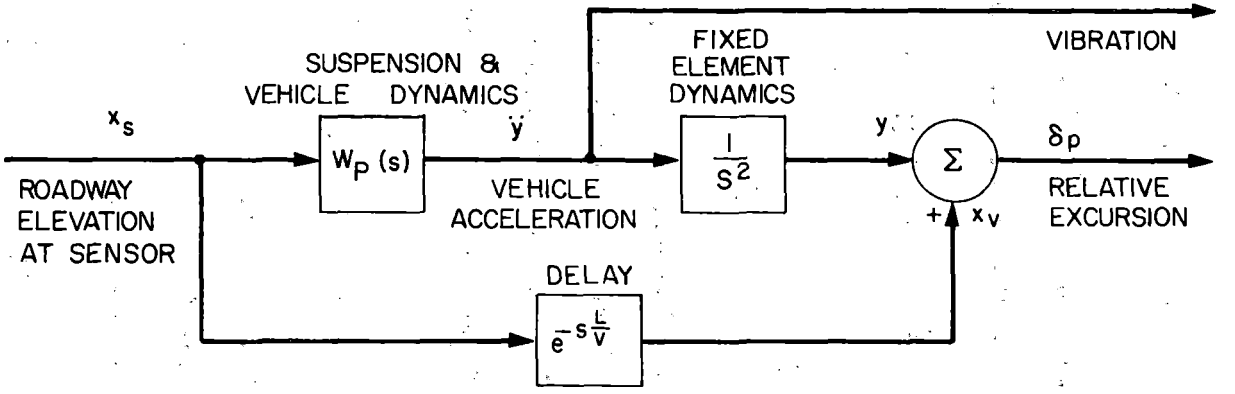

(b)

Figure 10. Preview Suspension System a) Schematic b) Block Diagram

Thus

$$\Gamma(s) = \frac{2\pi AV}{s^4} \tag{27}$$

$$\Delta(s) = 2\pi AV \frac{(\rho s^4 + 1)}{s^6} \tag{28}$$

$\Delta(s)$ may be factored into parts each of which contains only poles and zeroes in the right and left half planes as follows:

$$\Delta^-(s) = \frac{2\pi AV}{s^3} [\rho^{1/4}s - \frac{1}{\sqrt{2}}(1 + j)][\rho^{1/4}s - \frac{1}{\sqrt{2}}(1 - j)] \tag{29}$$

$$\Delta^+(s) = \frac{1}{s^3} [\rho^{1/4}s + \frac{1}{\sqrt{2}}(1 + j)][\rho^{1/4}s + \frac{1}{\sqrt{2}}(1 - j)] \tag{30}$$

When $\Gamma(s)/\Delta^-(s)$ is expanded in a sequence of partial fractions, the only term with poles in the left half plane is $1/s$. Consequently, $[\Gamma(s)/\Delta^-(s)]_+ = 1/s$ and, from Equations (24a) [Ref. 1] and (30), the synthesized suspension transfer function $W_p(s)$ is

$$W_p(s)_{L=0} = \frac{s^2}{\rho^{1/2}s + \sqrt{2}\rho^{1/4}s + 1} \tag{31}$$

The rms vehicle acceleration $\ddot{y}_{rms}$ and relative excursion $\delta_{p,rms}$ are found from Equations (1) and (31), Figure 10, and the tables corresponding to Equation (15) [Ref. 3]. Thus

$$\left.\frac{\ddot{y}^2_{rms}\rho^{3/4}}{2\pi AV}\right|_{L=0} = \frac{\sqrt{2}}{4} \tag{32}$$

$$\left.\frac{\delta^2_{p,rms}}{2\pi AV\rho^{1/4}}\right|_{L=0} = \frac{3\sqrt{2}}{4} \tag{33}$$

The weighting constant ρ may be eliminated from Equations (32) and (33)

to give the equation expressing the optimum zero preview vibration-clearance trade-off

$$\frac{\ddot{y}_{rms}}{\sqrt{2\pi AV}}\left[\frac{\delta_{rms}}{\sqrt{2\pi AV}}\right]^{3}_{L=0} = \frac{3\sqrt{3}}{8} \tag{34}$$

B. Infinite Preview

No system is likely to need-or would be capable of utilizing-profile information on the roadway very far (e.g., a one-hour travel time) in advance of the vehicle. However, the transfer function and trade-off curve for an infinite preview system are much easier to compute than those for a finite preview suspension and, in addition to giving ultimate performance limitations, present some interesting results not obtainable from finite preview considerations. Therefore, we may solve the Wiener-Hopf integral equation without regard to physical realizability restrictions (i.e., allow infinite preview). The Wiener-Hopf equation may be given by (8).

$$\Gamma(\tau) = \int_{-\infty}^{\infty} W_p(t)\Delta(\tau - t)dt \tag{35}$$

Multiplying each side of Equation (35) by $e^{-s\tau}$ and integrating over τ gives

$$\int_{-\infty}^{\infty} \Gamma(\tau)e^{-s\tau}d\tau = \int_{-\infty}^{\infty} e^{-s\tau}d\tau \int_{-\infty}^{\infty} W_p(t)\Delta(\tau - t)dt \tag{36}$$

or

$$\int_{-\infty}^{\infty} \Gamma(\tau)e^{-s\tau}d\tau = \int_{-\infty}^{\infty} W_p(t)e^{-st}dt \int_{-\infty}^{\infty} \Delta(\tau - t)e^{-s(\tau - t)}d\tau \tag{37}$$

Thus

$$\Gamma(s) = W_p(s)\Delta(s) \tag{38}$$

From Equations (11), (12) [Ref. 3], and (38), the expression for the optimum suspension transfer function for infinite preview $W_p(s)_{L=\infty}$ is

$$W_p(s)_{L=\infty} = \frac{H_1(-s)H_2(s)}{H_1(s)H_1(-s) + \rho} \tag{39}$$

The very remarkable feature of Equation (39) is that $W_p(s)_{L=\infty}$ is independent of the input. Consequently, one might suspect that a finite preview suspension system with characteristics similar to Equation (39) is likely to perform very well even for input signals with quite different statistics from those for which the system was synthesized. Before discussing finite preview control, let us find the vibration-clearance trade-off corresponding to Equation (39).

Since Equation (39) was derived by relaxing physical realizability constraints, $H_1(s) = 1/s^2$ and $H_2(s) = 1$, thus

$$W_p(s)_{L=\infty} = \frac{s^2}{\rho s^4 + 1} \tag{40}$$

By noting that $Y(s) = W_p(s)_{L=\infty} X(s)$ the expression for the rms value of $\ddot{y}$ is found from Equations (1), (15) [Ref. 3], and (40) as

$$\left[\frac{\ddot{y}^2_{rms}\rho^{3/4}}{2\pi AV}\right]_{L=\infty} = -\frac{1}{2\pi j}\int_{-j\infty}^{j\infty}\frac{\psi^2}{(\psi^4+1)^2}\,d\psi \tag{41}$$

where $\psi = \rho^{1/4}s$

Equation (41) may be evaluated from Appendix B for $x = 0$ and $n = 2$. Thus

$$\left[\frac{\ddot{y}^2_{rms}\rho^{3/4}}{2\pi AV}\right]_{L=\infty} = \frac{\sqrt{2}}{16} \tag{42}$$

Similarly, the rms relative excursion $\delta_{p,rms}$ found from Equations (1), (40) and $\delta_p(s) = (1 - W_p(s)/s^2)X(s)$ is

$$\left[\frac{\delta^2_{p,rms}}{2\pi AV\rho^{1/4}}\right]_{L=\infty} = -\frac{1}{2\pi j}\int_{-j\infty}^{j\infty}\frac{\psi^6}{(\psi^2+1)^2}\,d\psi \tag{43}$$

Equation (43) may also be evaluated from Appendix B for $x = 0$ and $n = 6$ as

$$\left[\frac{\delta^2_{p,rms}}{2\pi AV\rho^{1/4}}\right]_{L=\infty} = \frac{3\sqrt{2}}{16} \tag{44}$$

When ρ is eliminated from Equations (42) and (44), the vibration-clearance trade-off is described by

$$\frac{\ddot{y}_{rms}}{\sqrt{2\pi AV}}\left[\frac{\delta_{p,rms}}{\sqrt{2\pi AV}}\right]^3_{L=\infty} = \frac{3\sqrt{3}}{128} \tag{45}$$

Consequently, from the above and from Equation (34) the relation between vibration and clearance for infinite preview as compared with

zero preview for a roadway spectrum proportional to $1/\omega^2$ is

$$\frac{(\ddot{y}_{rms}\delta^3_{p,rms})_{L=\infty}}{(\ddot{y}_{rms}\delta^3_{p,rms})_{L=0}} = \frac{1}{16} \tag{46}$$

Thus, infinite preview provides a remarkable improvement over zero preview suspensions. Now that the potential of preview suspensions has been demonstrated, let us consider how suspension system improvement depends on the distance,L,ahead of the vehicle that the roadway is sensed.

C. Finite Preview

The method for synthesizing the optimum suspension transfer function for the case when a vehicle can sense the preceding roadway for a finite distance is similar to the steps taken for the zero preview situation. However, the delay shown in Figure 10b requires us to use a more rigorous and lengthy treatment. Until now we have merely divided double poles on the imaginary axis evenly into $\Delta^-(s)$ and $\Delta^+(s)$ when factoring $\Delta(s)$. Here, however, it is necessary to first shift any poles on the imaginary axis into the left or right half plane by very small amounts, ε_1 and ε_2 and then find limiting function values as ε_1 and ε_2 approach zero. Thus

$$\Phi_t(s) = \frac{AV}{(s + \varepsilon_1)(-s + \varepsilon_1)} \tag{47}$$

$$H_1(s) = \frac{1}{(s + \varepsilon_2)^2} \tag{48}$$

$$H_2(s) = e^{-sT} \tag{49}$$

From the above and Equations (11) and (12)[Ref. 3] the synthesizing functions $\Gamma(s)$ and $\Delta(s)$ are

$$\Gamma(s) = \frac{2\pi AVe^{-sT}}{(-s + \varepsilon_2)^2(s + \varepsilon_1)(-s + \varepsilon_1)} \tag{50}$$

$$\Delta(s) = \frac{2\pi AV(\rho s^4 - 2\varepsilon_2 \rho s^2 + \rho \varepsilon_2^4 + 1)}{(s + \varepsilon_2)^2(s + \varepsilon_1)(-s + \varepsilon_2)^2(-s + \varepsilon_1)} \tag{51}$$

For very small ε_2 the four roots of the numerator of Equation (51) lie well off the imaginary axis. For convenience then, let us approximate this numerator by $2\pi AV(\rho s^4 + 1)$. Thus, Equation (51) factors as follows:

$$\Delta^-(s) = \frac{2\pi AV[\rho^{1/4}s - \frac{1}{\sqrt{2}}(1 + j)][\rho^{1/4}s - \frac{1}{\sqrt{2}}(1 - j)]}{(-s + \varepsilon_2)^2(-s + \varepsilon_1)} \tag{52}$$

$$\Delta^+(s) = \frac{[\rho^{1/4}s + \frac{1}{\sqrt{2}}(1 + j)][\rho^{1/4}s + \frac{1}{\sqrt{2}}(1 - j)]}{(s + \varepsilon_2)^2(s + \varepsilon_1)} \tag{53}$$

Dividing Equation (50) by Equation (52) gives

$$\frac{\Gamma(s)}{\Delta^-(s)} = \frac{e^{-sT}}{(s + \varepsilon_1)[\rho^{1/4}s - \frac{1}{\sqrt{2}}(1 + j)][\rho^{1/4}s - \frac{1}{\sqrt{2}}(1 - j)]} \tag{54}$$

The inverse Fourier transform of $\Gamma(s)/\Delta^-(s)$ is a time function $\gamma(t)$ which generally has non-zero values for plus and minus t.

The function $[\Gamma(s)/\Delta^{-}(s)]_{+}$ is the Fourier transform of $\gamma(t)$ for $t > 0$. Thus far it has been possible to find $[\Gamma(s)/\Delta^{-}(s)]_{+}$ by expressing $\Gamma(s)/\Delta^{-}(s)$ in a partial fraction expansion and retaining only terms with poles in the left half plane. Since $\Gamma(s)/\Delta^{-}(s)$ in Equation (54) is a transcendental function, $[\Gamma(s)/\Delta^{-}(s)]_{+}$ is evaluated first by finding $\gamma(t)$ and then by taking the Laplace transform of $\gamma(t)$ which is identical in form to the Fourier transform of $\gamma(t)$ for $t > 0$. Thus

$$\gamma(t) = \frac{1}{2\pi j} \int_{-j\infty}^{j\infty} e^{st} \frac{\Gamma(s)}{\Delta^{-}(s)} \, ds \tag{55}$$

From Equations (54) and (55)

$$\gamma(t) = \frac{1}{2\pi j} \int_{j\infty}^{j\infty} \frac{e^{s(t-T)}}{(s + \varepsilon_1)[\rho^{1/4}s - \frac{1}{\sqrt{2}}(1 + j)][\rho^{1/4}s - \frac{1}{\sqrt{2}}(1 - j)]} \tag{56}$$

Equation (56) is evaluated in two parts (see Figure 11a). First, for a path of integration around the left half plane, corresponding to $(t-T) > 0$, $\gamma(t)$ is equal to the residue at $s = -\varepsilon_1$. Secondly, for $(t-T) < 0$, $\gamma(t)$ is equal to minus the sum of the residues at poles (a) and (b) for a contour taken clockwise around the right half plane. The residue at $-\varepsilon_1$ is

$$\text{Res}(-\varepsilon_1) = \frac{e^{-\varepsilon_1(t-T)}}{\rho^{1/2}\varepsilon_1^{\,2} + \sqrt{2}\,\rho^{1/4}\,\varepsilon_1 + 1} \tag{57}$$

Taking the limit as $\varepsilon_1 \to 0$ gives

$$\gamma(t) = 1 \qquad \text{For } (t-T) > 0 \tag{58}$$

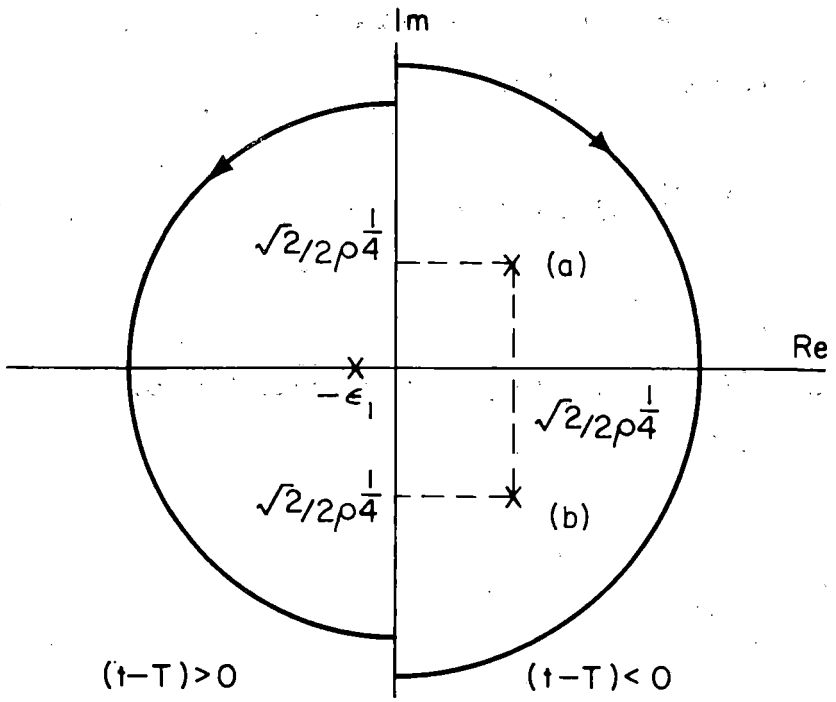

(a)

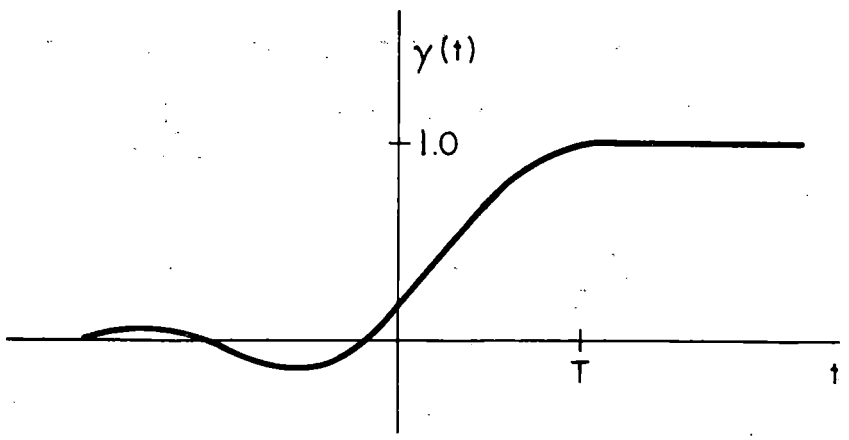

(b)

Figure 11. a) Contour Integration of $\Gamma(s)/\Delta^{-}(s)$ b) Inverse Fourier Transform of $\Gamma(s)/\Delta^{-}(s)$

By evaluating the residues of the poles at (a) and (b), $\gamma(t)$ for $(t - T) < 0$ becomes (see Figure 10b)

$$\gamma(t) = e^{(t-T)/\tau}\, 1[\cos\left(\frac{t-T}{\tau}\right) - \sin\left(\frac{t-T}{\tau}\right)] \qquad \text{For } (t-T) > 0 \qquad (59)$$

where $\tau = \sqrt{2}\,\rho^{1/4}$.

The function $[\Gamma(s)/\Delta^{-}(s)]_{+}$ may now be evaluated by taking the Laplace transform of $\gamma(t)$ as follows:

$$\frac{\Gamma(s)}{\Delta^{-}(s)_{+}} = \int_0^{\infty} \gamma(t) e^{-st} dt \qquad (60)$$

From Equations (59) and (60) we have

$$\frac{\Gamma(s)}{\Delta^{-}(s)_{+}} = \int_0^{T} e^{(t-T)/\tau}[\cos(\frac{t-T}{\tau}) - \sin(\frac{t-T}{\tau})]e^{-st} dt + \int_T^{\infty} e^{-st} dt \qquad (61)$$

When the above integration is carried out and $[\Gamma(s)/\Delta^{-}(s)]_{+}$ is divided by $\Delta^{+}(s)$ (Equation (53)), the expression for the synthesized finite preview suspension transfer function $W_p(s)_{L=L_o}$ is

$$W_p(s)_{L=L_o} = \frac{s^2(A_1\rho^{1/2}s^2 - \sqrt{2}A_2\rho^{1/4}s + 1)}{\rho s^4 + 1} \qquad (62)$$

where $A_1 = e^{-T/\tau}(\cos T/\tau + \sin T/\tau)$

$A_2 = e^{-T/\tau}(\cos T/\tau)$

The rms acceleration and clearance may be found from Equation (62), and the relations indicated by Figure 10. Thus

$$\left.\frac{\ddot{y}^2_{rms}\rho^{3/4}}{2\pi AV}\right|_{L=L_o} = \frac{1}{2\pi j}\int_{-j\infty}^{j\infty} \frac{-\psi^2(A_1\psi^2 - \sqrt{2}\,A_2\psi + e^{-\psi T/\rho^{1/4}})}{(\psi^4+1)^2} \cdot \frac{(A_1\psi^2 + \sqrt{2}\,A_2\psi + e^{\psi T/\rho^{1/4}})}{1}\,d\psi \qquad (63)$$

When the numerator of the integrand in Equation (63) is reduced, there will be some terms of the form

$$\psi^n e^{-\psi T/\rho^{1/4}}/(\psi^4+1)^2$$

By replacing ψ with $-\psi$ and appropriately adjusting integration limits, Equation (63) becomes

$$\left[\frac{\ddot{y}^2_{rms}\rho^{3/4}}{2\pi AV}\right]_{L=L_o} = \frac{1}{2\pi j}\int_{-j\infty}^{j\infty} \frac{-A_1{}^2\psi^6 - 2A_1 e^{\psi T/\rho^{1/4}} + 2A_2\psi^4 + 2\sqrt{2}A_2 e^{\psi T/\rho^{1/4}}\psi^3 - \psi^2}{(\psi^4+1)^2}\,d\psi \qquad (64)$$

When Equation (64) is evaluated (see Appendix B), we have

$$\left[\frac{\ddot{y}^2_{rms}\rho^{3/4}}{2\pi AV}\right]_{L=L_o} = \frac{\sqrt{2}}{16}(A_1{}^2 + 4A_1{}^2T/\tau + 2A_2{}^2 + 1) \qquad (65)$$

In an entirely similar manner, the expression for the relative excursion is found as

$$\left[\frac{\delta^2_{p,rms}}{(2\pi AV\rho)\,1/4}\right]_{L=L_o} = \frac{\sqrt{2}}{16}\,(3 + 3a_1^2 - 4A_1^2 T/\tau + 6A_2^2) \qquad (66)$$

The trade-off curves between rms acceleration and clearance space ($h_p = 2\alpha\delta_{p,rms}$) are plotted in Figure 12 for several values of preview time (in seconds) along with curves for zero and infinite preview [Equations (34) and (45)].

The relationship between the benefits that may be brought about by preview control and preview time are not apparent from Figure 12. Consequently, let us pick a design point on the zero preview line ($h/2\alpha\sqrt{2\pi AV} = 0.4$, $\ddot{y}_{rms}/\sqrt{2\pi AV} = 10.0$) and determine how $\ddot{y}_{rms}$ may be reduced for constant h and AV, how h may be reduced for constant $\ddot{y}_{rms}$ and AV, and how AV may be increased for constant $\ddot{y}_{rms}$ and h. The results shown in Figure 13 indicate that substantial reductions in vibrations and clearance space may be brought about by using preview control. For a given vibration and clearance space a vehicle using preview control may travel up to four times faster or over a road four times rougher (as measured by A) than one without preview.

D. Step Response

A great deal of insight into the nature of preview suspensions may be gained from the step response (y/x) plots of these systems. First, because of the analogy between the integral square and mean square of response variables subjected respectively to step inputs

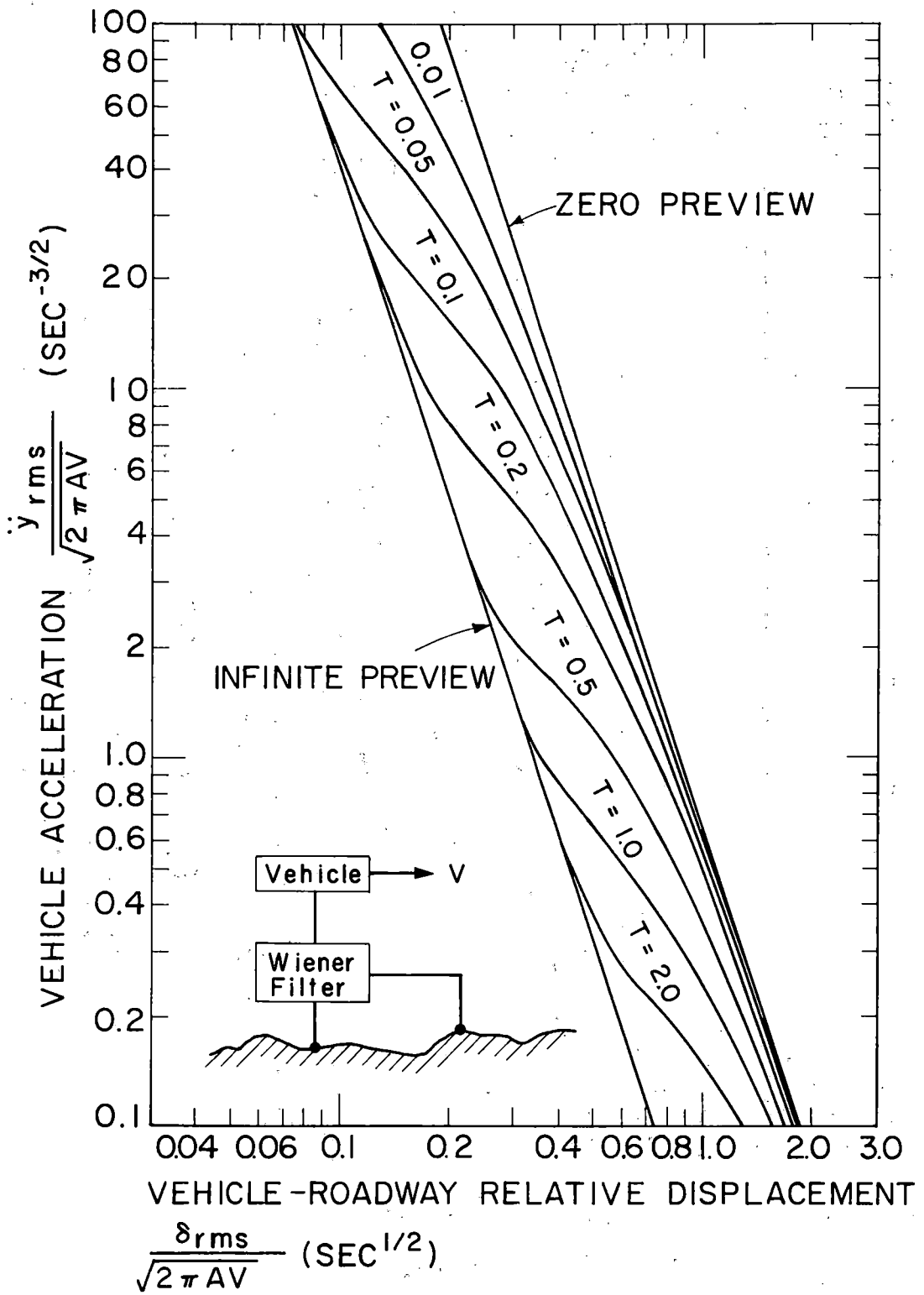

Figure 12. Vibration - Clearance Trade - Off for Synthesized Suspension for Several Values of Preview Time, T, (Seconds)

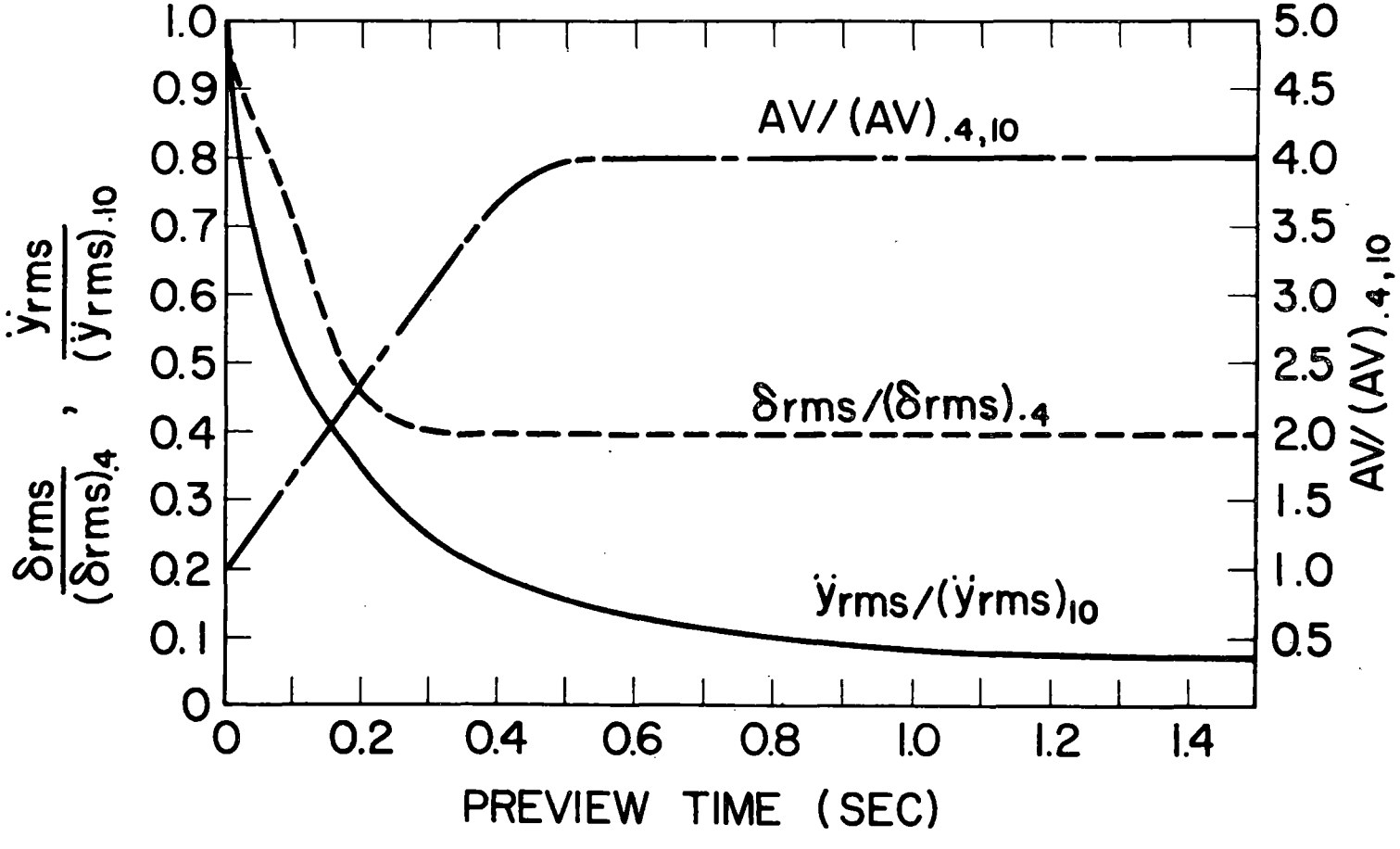

Figure 13. Example of Improvements in Speed Capabilities, Clearance Space, and Sprung Mass Acceleration as a Function of Preview Time for Synthesized Suspensions

and random inputs of the form AV/s^2 (see Appendix C) a qualitative comparison may be made among systems which operate with various preview times. Furthermore, step response plots facilitate a physical interpretation of the capabilities of preview systems which function with less acceleration and less relative excursion than optimum non-preview suspensions. Finally, step response plots provide hints for the development of systems which might be easily mechanized and which perform nearly as well as optimum synthesized preview suspensions.

The response of vehicle position y to a step in roadway elevation x_s is found from the definition of the inverse Fourier transform and the transfer function $W_p(s)$ [Equation (62)] by noting that $Y/X = W_p(s)/s^2$. Thus

$$y_s(t) = \lim_{\varepsilon \to 0} \int_{-j\infty}^{j\infty} \frac{A_1 \rho^{1/4} s^2 - \sqrt{2}\, A_2 \rho^{1/4} s + e^{-sT}}{(s + \varepsilon)(\rho s^4 + 1)}\, e^{st} ds \qquad (67)$$

When the integration in the above equation is carried out, the step response $y_s(t)$ is found as

$$y_s(t) = \frac{1}{2} + \frac{1}{2}\,\frac{t - T}{t - T}\left[1 - e^{-\frac{t-T}{\tau}} \cos\left(\frac{t - T}{\tau}\right)\right]$$

$$- \frac{1}{2}\, e^{-\left(\frac{t+T}{\tau}\right)} \left[\cos\left(\frac{t - T}{\tau}\right) + 2 \sin\left(t/\tau\right)\cos\left(T/\tau\right)\right] \qquad (68)$$

Equation (68) is plotted in Figure 14 for several values of preview time T from the point of view of an observer at the vehicle. Thus, preview time is the distance from $t/\tau = 0$ to the beginning of the

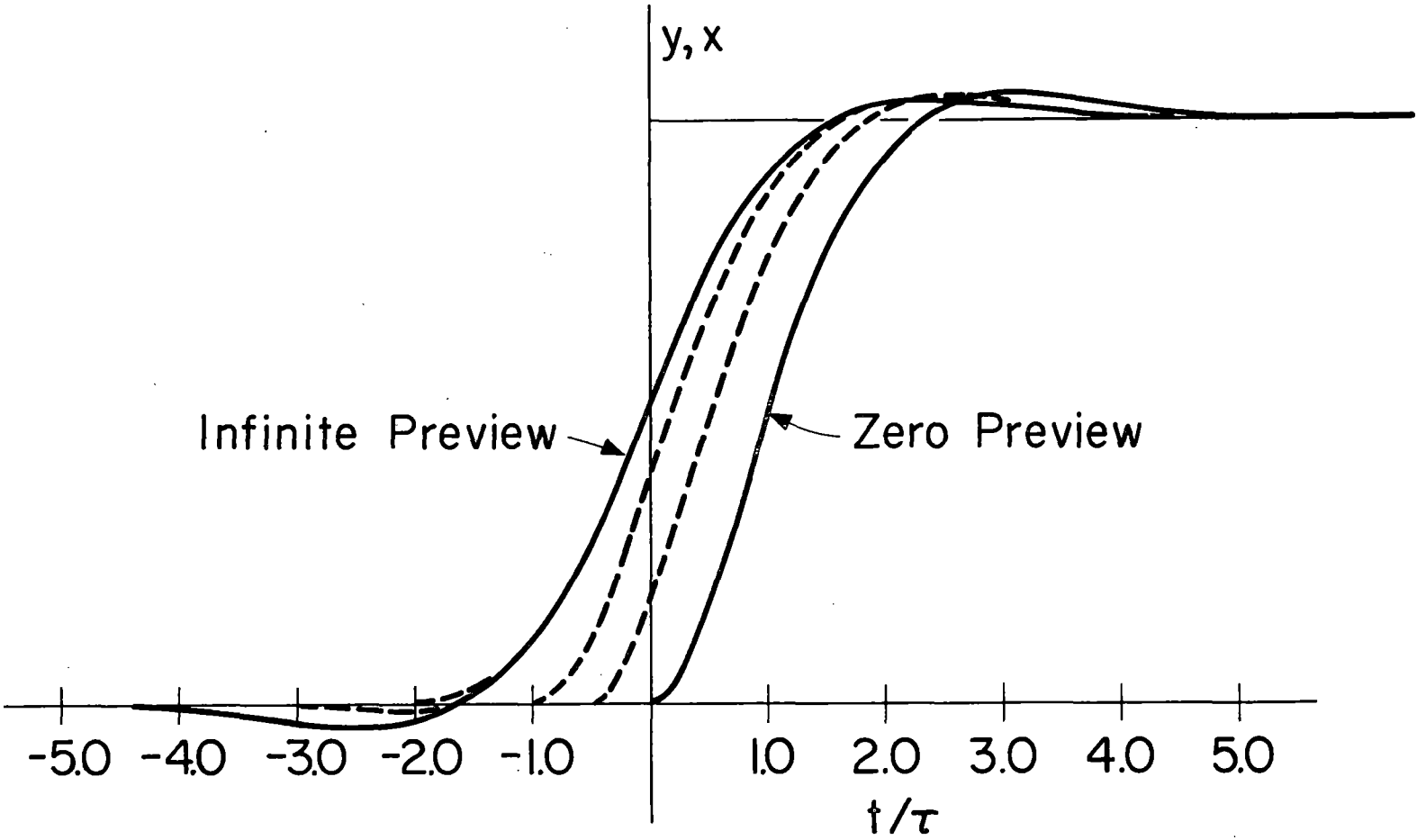

Figure 14. Synthesized Suspension Step Responses (y/x) for Several Values of Preview Time

response. The non-dimensionalizing parameter $\tau = \sqrt{2}\,\rho^{1/4}$ may be thought of as a scaling factor. For example, when acceleration is to be small, ρ, hence τ, is large. Consequently, the step responses are more gradual than they would be if more importance were given to relative excursion.

Figure 14 shows how preview control improves both acceleration and relative excursion. Acceleration is proportional to the curvature (second derivative) of the plots in Figure 14 and relative excursion is proportional to the difference between the step and a response curve. The rms criterion weighs variables more heavily for large values than for small. Consequently, the zero preview step response shows that a large initial relative displacement and curvature will contribute to considerable rms excursion and acceleration. As longer preview time is used, response curves become more gradual and result in smaller relative displacement as the vehicle body responds to a step in roadway elevation before actually reaching it.

E. Mechanization of Preview Control

Mechanization of the transfer function for the optimum preview suspension [Equation (62)] is not at all straightforward. Since some of the poles of Equation (62) lie in the right half plane, the system response first diverges then converges as illustrated by the infinite preview step response in Figure 14. Consequently, the approach taken here is to examine the step responses in Figure 14 and devise systems with similar responses.

The equation for infinite preview [Equation (40)] is

identical in form to that for an infinite beam on an elastic foundation [9]. (The static deflection equation for a beam on an elastic foundation may be derived by minimizing the weighted sum of the integral of curvature squared plus deflection squared which is analagous to minimizing the weighted sum of rms acceleration plus relative excursion.) Consequently, one suspects that the steady state behavior of a very long train such as that proposed by Edwards [10] might approach that of an optimum preview system. However, this is a very restricted case.

Let us determine the capabilities of the general, but elementary, model of the preview suspension system illustrated schematically in Figure 15. The vehicle, idealized as a rigid mass, is supported above the roadway by a suspension of stiffness, k_v. The spring, k_s, represents a simple preview controller in which a force applied to the vehicle is proportional to the difference between the vehicle position, y, and elevation, x_s, of the roadway in front of the vehicle. Damping is proportional to vehicle velocity as shown by a damper attached to an inertial reference. In practice this form of damping could be approximated by generating a suspension force proportional to the integral of the output of a vehicle-mounted accelerometer.

The position transfer function Y/X for the system shown in Figure 15 is

$$\frac{Y}{X_s}(s) = \frac{k_s + k_v e^{-sT}}{Ms^2 + cs + k_v + k_s} \tag{69}$$

Equation (69), rewritten in terms of nondimensional variables is

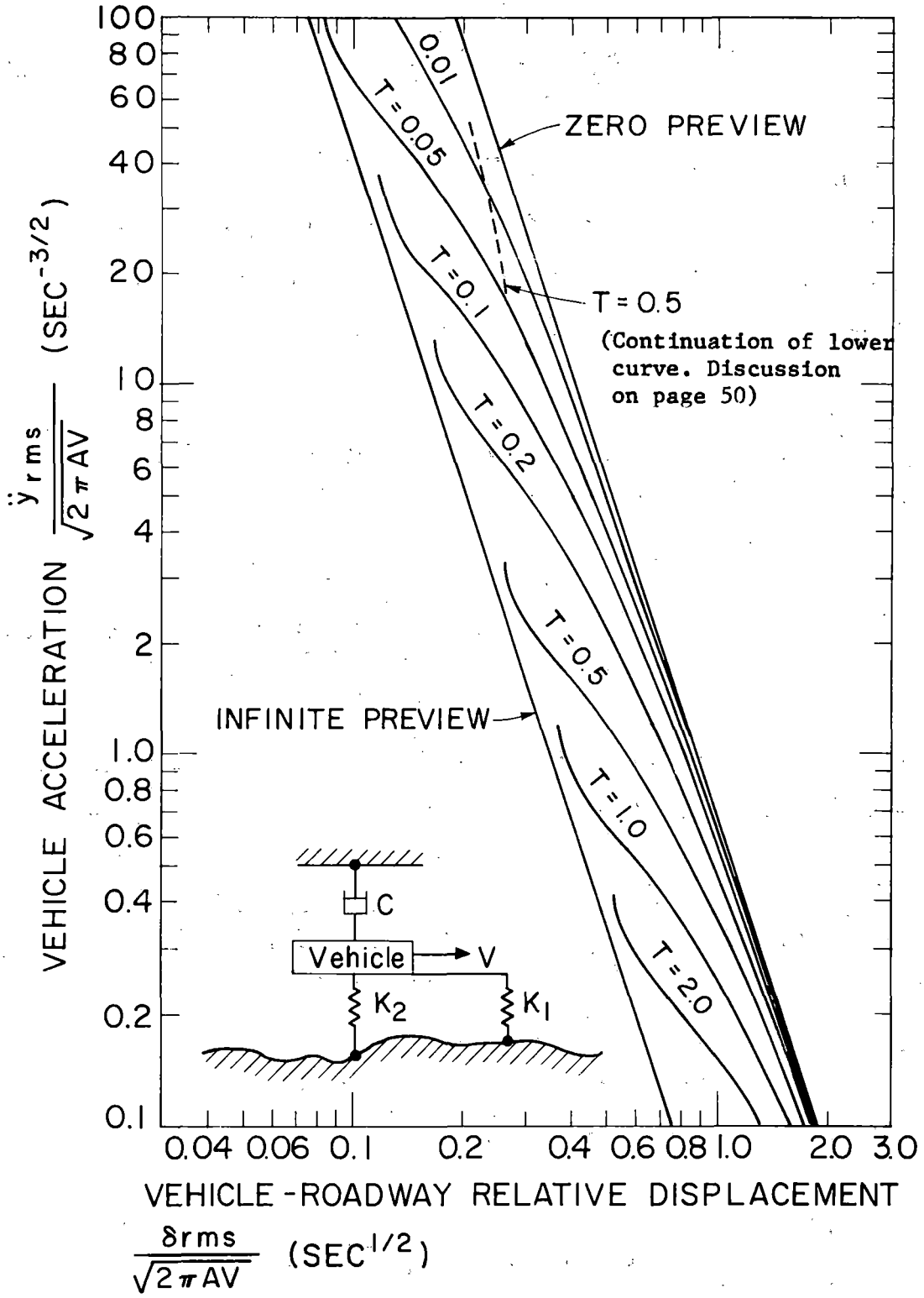

Figure 15. Vibration - Clearance Trade - Off for Simple Preview Suspension for Several Values of Preview Time, T, (Seconds)

$$\frac{Y}{X_s}(s) = \frac{a + (1 - a)e^{-\phi\omega_n T}}{\phi^2 + 2\zeta\phi + 1} \tag{70}$$

where $\omega_n^2 = (k_v + k_s)/M$, $\zeta = c/2\sqrt{(k_v + k_s)M}$, $\phi = s/\omega_n$ and "a" which is a measure of distribution of stiffness between k_v and k_s is $k_s/(k_v + k_s)$. From Equations (47) (with $\varepsilon_1 = 0$) and (70), the expression for the rms vehicle acceleration is

$$\frac{\ddot{y}^2_{rms}}{2\pi AV} = \frac{\omega_n^3}{2\pi j} \int_{-j\infty}^{j\infty} \frac{-\phi^2[1 - 2a + 2a^2 + a(1 - a)e^{\phi\omega_n T}]}{(\phi^2 + 2\zeta\phi + 1)(\phi^2 - 2\zeta\phi + 1)} d\phi$$

$$+ \frac{\omega_n^3}{2\pi j} \int_{-j\infty}^{j\infty} \frac{-\phi^2 a(1 - a)e^{-\phi\omega_n T}}{(\phi^2 + 2\zeta\phi + 1)(\phi^2 - 2\zeta\phi + 1)} d\phi \tag{71}$$

Equation (71) may be simplified by replacing ϕ with $-\phi$ in the second integral and appropriately adjusting limits of integration to give

$$\frac{\ddot{y}_{rms}}{2\pi AV} = \frac{\omega_n^3}{2\pi j} \int_{-j\infty}^{j\infty} \frac{\phi^2[-1 + 2a(1 - a)(1 - e^{\phi\omega_n T})}{(\phi^2 + 2\zeta\phi + 1)(\phi^2 - 2\zeta\phi + 1)} d\phi \tag{72}$$

When the above integral is evaluated (see Appendix D), the expression for rms acceleration is

$$\frac{\ddot{y}^2_{rms}}{2\pi AV} = \frac{\omega_n^3}{4\zeta} \quad 1 + 2a(1 - a)[-1 + e^{-\zeta\omega_n T}(\cos\sqrt{1 - \zeta^2}\,\omega_n T$$

$$- \frac{\zeta}{\sqrt{1 - \zeta^2}} \sin\sqrt{1 - \zeta^2}\,\omega_n T)] \tag{73}$$

The root mean square of the relative displacement of the vehicle with respect to the roadway is given by

$$\delta_p(s) = X_v(s) - Y(s) \tag{74}$$

Thus, since $X_v(s) = X_s(s)e^{-sT}$

$$\frac{\delta_p}{X}(s) = \frac{(\phi^2 + 2\zeta\phi + a)e^{-\phi\omega_n T} - a}{\phi^2 + 2\zeta\phi + 1} \tag{75}$$

From Equations (47) and (75), the expression for $\delta_{p,rms}$ is given by

$$\frac{\delta^2_{p,rms}\,\omega_n}{2\pi AV} =$$

$$\frac{1}{2\pi j}\int_{-j\infty}^{j\infty} \frac{\phi^4+2(a-2\zeta^2)\phi^2-2a\phi^2 e^{\phi\omega_n T}+4a\zeta\phi e^{\phi\omega_n T}+2a^2(1-e^{\phi\omega_n T})}{(\phi+\epsilon_1)(\phi^2+2\zeta\phi+1)(-\phi+\epsilon_1)(\phi^2-2\zeta\phi+1)}\,d\phi \tag{76}$$

When the above integral is evaluated (see Appendix D), the expression for $\delta_{p,rms}$ becomes

$$\frac{\delta^2_{rms}}{2\pi AV} = \frac{1}{4\zeta\omega_n}\Big[1 - 2(a - 2\zeta^2) - 2a^2(4\zeta^2 - 1) + 2a[1 - a + 4\zeta^2(1 + a)]e^{-\zeta\omega_n T}\cos\sqrt{1 - \zeta^2}\,\omega_n T + 2a\zeta\Big[-1 + \zeta^2(1 + a) - 3a\Big]\frac{e^{-\zeta\omega_n T}}{\sqrt{1 - \zeta^2}}\sin\sqrt{1 - \zeta^2}\,\omega_n T - \frac{2a\zeta}{\omega_n} + a^2 T\Big] \tag{77}$$

The values of parameters a, ζ, and ω_n, which optimize the trade-off between vibration and clearance space, are found by minimizing $P = \rho \ddot{y}_{rms} + \delta_{p,rms}$. The trade-off curves resulting from a digital computer parameter search (see Appendix A) are illustrated in Figure 15. These curves overlap the optimum synthesized trade-off curves shown in Figure 12 except near the infinite preview line. In this region the curves bend away from those corresponding to the synthesized suspension and terminate. At these end points a = 1.0 indicating that the spring beneath the vehicle has zero stiffness. Consequently, the step response, from the point of view of an observer on the vehicle, is that of a simple spring-mass-damper system but advanced by a time T. The only way a smaller value of clearance may be obtained for this model is by having a relatively flexible preview controller spring (small k_s) and a stiff suspension spring (large k_v). This combination results in a system which allows small clearance space only at the expense of very high acceleration levels. The dotted curve for T = 0.5 seconds, shown in Figure 15, indicates this aspect quantitatively. It is difficult to imagine a situation in which such a system would be desirable since better performance may be achieved with shorter preview times.

The presence of the discontinuity in trade-off curves is illustrated by a contour plot (Figure 16) of P as a function of "a" and ω_n for $\zeta = 0.7$, and T = 0.5. The minimum at a = 1.0 corresponds to the lower solid curve in Figure 15 whereas the minimum at a = .15 represents the higher dotted line. The large value for the natural frequency ω_n at the latter minimum explains the large acceleration levels found for the upper portion of the T = 0.5 seconds trade-off curve.

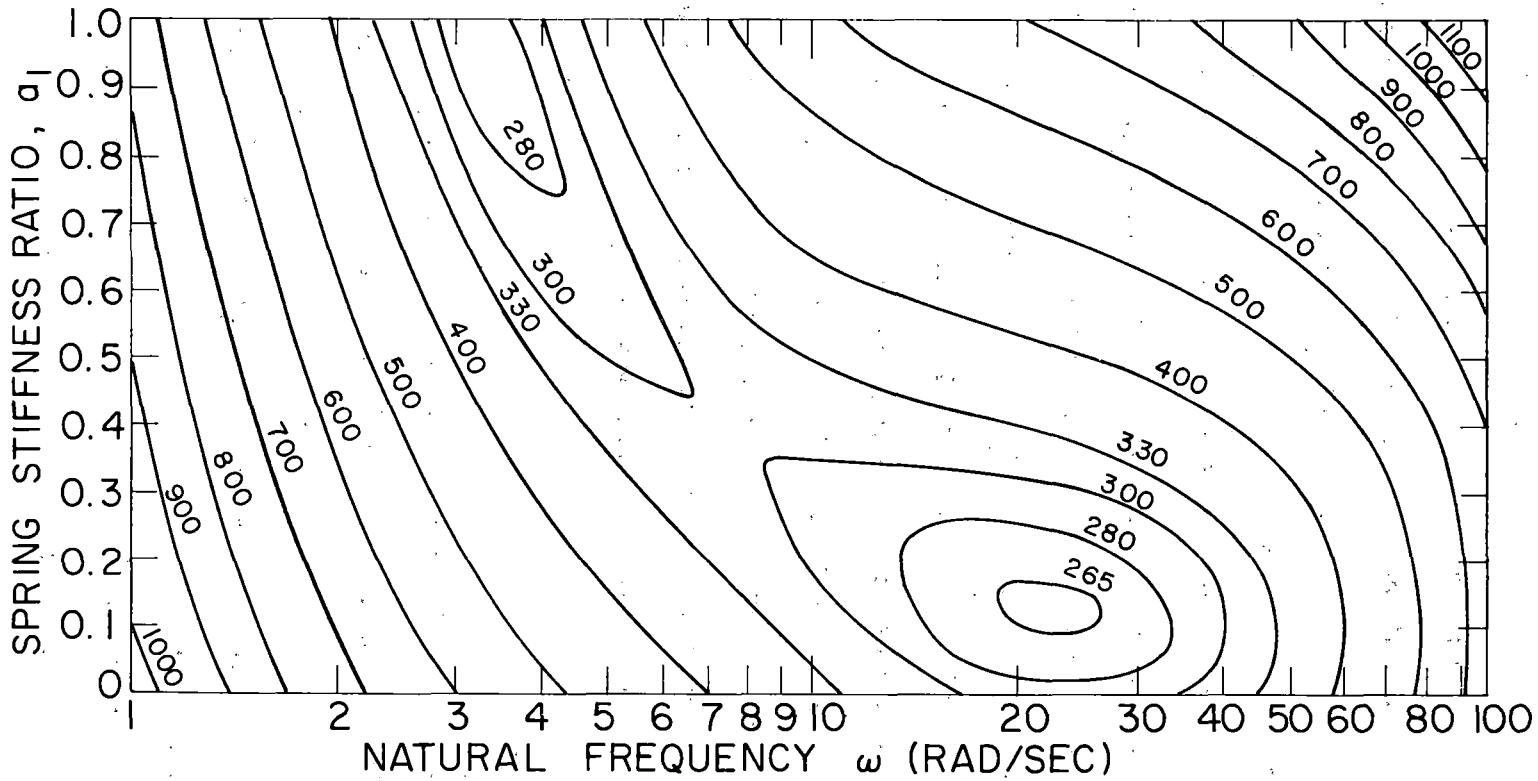

Figure 16. Penalty Function Contour Plot for $\zeta = 0.7$ and $T = 0.5$ for Simple Preview Suspension

V. NUMERICAL EXAMPLE

The preceding sections have presented rather general discussions of the optimization of the random vibration characteristics of vehicle suspensions. In order to illustrate the use of some of the suspension design charts (Figures 3, 8, and 9), a numerical example will be considered. First, a preliminary design of a conventional spring-shock absorber suspension will be carried out with the aid of Figure 3 for a high speed ground vehicle. Performance benefits that might be brought about by using automatic height control or synthesized suspensions will be examined. Figure 8 will be used to determine whether the suspensions thus far considered possess adequate road holding qualities. From Figure 9 we will establish a fundamental limitation to the primary design chart (Figure 3). Finally, the frequency responses, power spectral densities, and time responses to random roadway inputs will be found for several possible preliminary designs.

A. Use of Design Charts

The problem posed is to do a preliminary design study of a suspension system for a vehicle traveling 200 mph over a medium quality highway, $A = 2 \times 10^{-5}$ ft. First, in order to establish a design vibration level, let us compute the rms acceleration of an automotive type of vehicle going 70 mph over the same highway. For $\zeta = 0.5$, $r = 0.1$, $f_u = 10$ Hz, and $f_s = \sqrt{k_{12}/M}\,/2\pi = 1.5$ Hz the automobile sprung mass vibration is about 5.5 ft/sec^2.*

* Passengers would not feel this vibration level because seats filter much of the acceleration.

Let us suppose for the high speed vehicle that r = 0.1, f_u = 10 Hz, α is equal to 3 to insure that bottoming occurs very infrequently and that loading variations are equal to 75% of the weight of the sprung mass. From these data, the nondimensional loading variations are

$$\ddot{y}_{rms}/4\pi^2\sqrt{AVf_u^3} = 0.056 \tag{78}$$

$$= F/8\pi^2\alpha M\sqrt{AVf_u^3} = 0.05 \tag{79}$$

Thus, in Figure 3 Equation (78) is satisfied at point "a" on the = 0.05 line and

$$(h/2\alpha)\sqrt{f_u/AV} = 9.0 \tag{80}$$

Therefore, the design clearance is

$$h = 1.31 \text{ ft.} \tag{81}$$

The design chart also shows that, at the design point "a", the optimum parameter values are

$$\zeta = 0.2$$

$$f_s = 1.0 \text{ Hz} \tag{82}$$

A 1.31 ft. suspension clearance seems rather large. If a low frequency automatic height control system were used to compensate for loading variations, F/k = 0 and the = 0 line applies. Point b in Figure 3 indicates that the suspension clearance would have to be only 5.25 inches if the same vibration level were maintained. Point c shows that the minimum possible clearance space is about 4.1 inches for the

optimum synthesized suspension. Thus,for this case an automatic height control suspension provides a suspension with nearly optimum performance.

If a 1.31 ft. suspension clearance is acceptable, then Figure 3 shows that active systems may be incorporated to reduce vibration and provide a more comfortable ride. Points d and e indicate that an automatic height controller and optimum synthesized suspension may reduce sprung mass vibration by factors of 3 and 7-1/2, respectively. In this case, it appears that an optimum synthesized suspension offers a significant advantage over an automatic height controller which, in turn, is considerably more effective than a simple spring-shock absorber suspension.

Although the above discussion is valuable in comparing the vibration-clearance aspects of several suspensions, we must investigate further to determine whether the suspensions cited provide adequate wheel-road contact. From Equation (12), the static unsprung mass deflection δ_o is .09 ft. Since the rms relative wheel-roadway excursion δ_w should be at least three times smaller than δ_o, the maximum allowable value for δ_w is .03 ft. Thus

$$(\delta_w \sqrt{f_u/AV})_{max} = 1.4 \tag{83}$$

The points a - e in Figure 10 correspond to those in Figure 3. Only three points, a , b , and c , fall below the 1.4 ordinate of Figure 6. Hence the suspensions corresponding to these points provide adequate wheel-road contact; whereas those suspensions corresponding to points d and e are unacceptable due to large wheel-roadway excursions.

Figure 8 may be used to determine the minimum possible vibration isolation capabilities of a linear suspension which maintains nearly continuous wheel-roadway contact. The numerical value of the abscissa, using the above high speed vehicle parameters, is

$$\frac{f_u^3 AV}{g^2} = 0.0058 \tag{84}$$

From Figure 8 the minimum rms suspension force is

$$\frac{F_{rms}}{(m + M)g} = 0.118 \tag{85}$$

Since $\ddot{y}_{rms} = F_{rms}/M$, the minimum point on the ordinate of Figure 3 becomes

$$\frac{\ddot{y}_{rms}}{4\pi\sqrt{AVf_u^3}} = 0.043 \tag{86}$$

Thus, the largest vibration reduction from points a, b, and c that might be brought about is only 23%.

B. Frequency Responses and Power Spectral Densities

Of the five optimum systems, a-e, originally considered only three, a, b, and c, met the road holding constraint. The vehicle acceleration, sprung mass-unsprung mass relative excursion and the unsprung mass-roadway relative excursion frequency responses and power spectral densities for these three designs, illustrated in Figure 17, show at least two significant factors. First, as may be

seen by comparing frequency responses and power spectral densities for each variable, the $1/\omega^2$ form of roadway elevation spectra causes considerably greater spectral content at the low frequency range than might be expected by merely inspecting frequency response plots. Secondly, active systems tend to attenuate or shift to higher frequencies the low frequency peak of the conventional spring-shock absorber suspension.

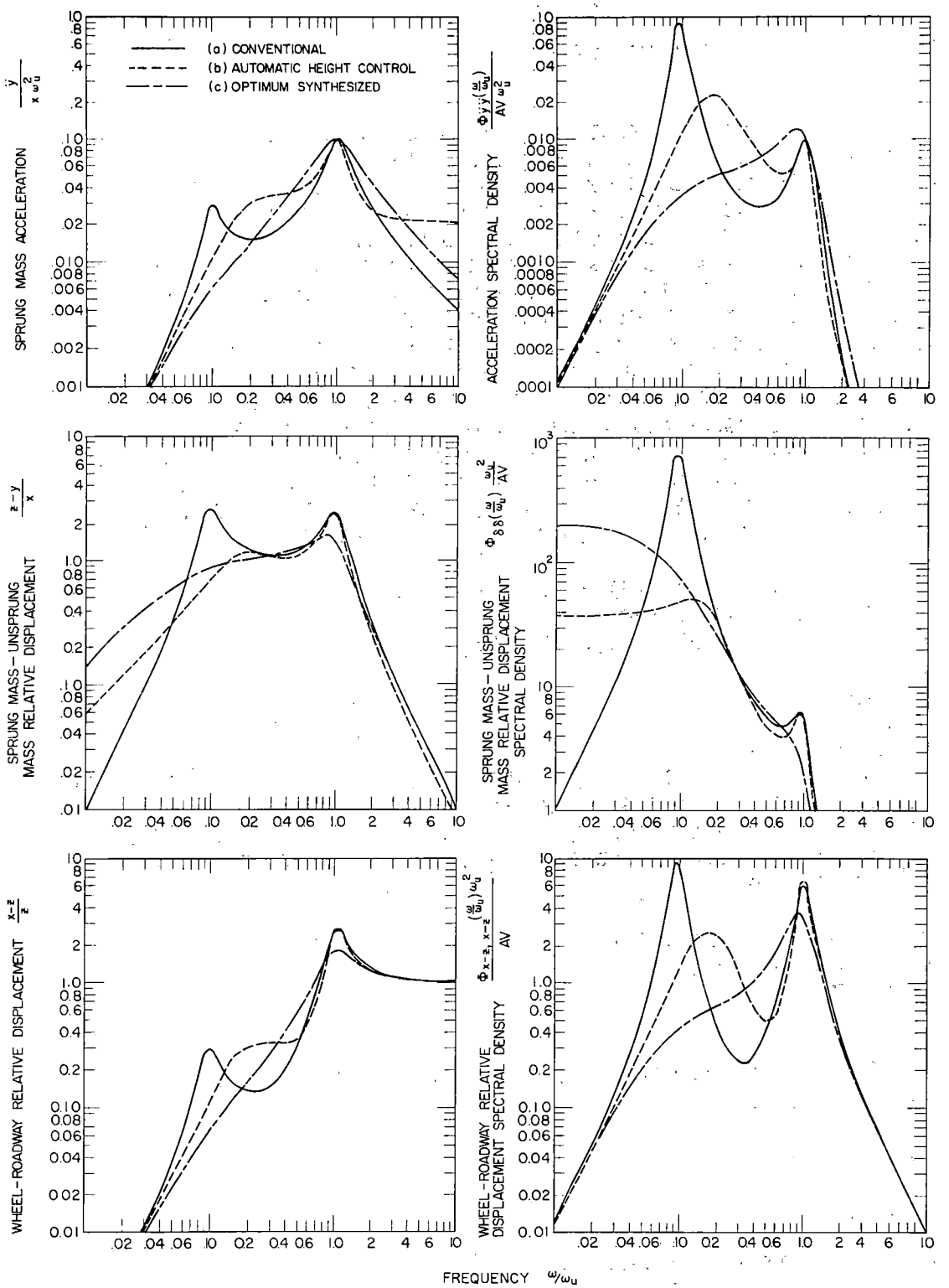

Figure 17. Acceleration, Sprung Mass - Unsprung Mass Excursion, and Wheel - Roadway Excursion Frequency Responses and Power Spectral Densities Corresponding to Systems a, b, and c in Figure 6

APPENDIX A

MINIMIZATION PROGRAM

```
C  THIS PROGRAM, WRITTEN IN FORTRAN 4, IS USED TO MINIMIZE A FUNCTION OF
C  I VARIABLES B(I) USING A HILL CLIMBING TECHNIQUE. THE PROGRAM EVALUATES
C  A FUNCTION F IN THE MIDDLE OF A BOUNDED SECTION OF PARAMETER SPACE
C  THEN INCREMENTS EACH PARAMETER PLUS AND MINUS 10 PERCENT OF ITS MAXIMUM
C  RANGE, EVALUATING THE FUNCTION AT EACH STEP. WHENEVER A VALUE OF THE
C  FUNCTION IS FOUND THAT IS LESS THAN THE STARTING VALUE, FO, THE PROGRAM
C  CONTINUES FROM THE NEW POINT. WHEN A POINT IN PARAMETER SPACE IS
C  REACHED SUCH THAT THE FUNCTION VALUE CORRESPONDING TO THAT POINT IS
C  LESS THAN THE VALUES OF THE FUNCTION CORRESPONDING TO THE POINTS
C  DETERMINED BY PLUS AND MINUS INCREMENTS OF EACH PARAMETER THE INCREMENT
C  OR JUMP SIZE IS REDUCED BY A FACTOR OF TEN AND THE SEARCH PROCESS IS
C  CONTINUED. THE PROGRAM GIVEN HERE IS FOR THREE PARAMETERS AND EIGHT
C  ITERATIONS. HOWEVER, IT MAY BE EASILY CHANGED FOR OTHER NUMBERS OF
C  PARAMETERS AND ITERATIONS. THE BOUNDS ON THE PARAMETER SPACE ARE
C  GIVEN BY A(J) = BMAX(J), C(J) = BMIN(J). THE SUBROUTINE SHOOT IS FOR
C  THE FIXED CONFIGURATION PREVIEW CONTROL OPTIMIZATION.

      DIMENSION D(3),B(3),C(3),BO(3),DLB(3),A(3)
      COMMON DELRMS,ACCEL,RHO,T
      READ(5,2) A(1),A(2),A(3),C(1),C(2),C(3)
    2 FORMAT(7F10.5)
    3 READ(5,5)T,RHO
    5 FORMAT(2F15.8)
      WRITE(6,200)
  200 FORMAT(104H1        T            RHO            A1     NATL FRQ (W) DA
     1MP RATIO (Z)  DELTA RMS  ACCEL RMS         FO     /)
C     SET UP INITIAL VALUES OF B(I), JUMP SIZE DLB(J), AND PARAMETER
C     D(J) WHICH IS USED TO INDICATE WHEN ALL VARIABLES ARE WITHIN ONE
C     JUMP OF THE OPTIMUM
      DO 6 J=1,3
      DLB(J) = 0.1*(A(J)-C(J))
      B(J) =0.5*(A(J)+C(J))
    6 CONTINUE
      CALL SHOOT(F,B)
      FO = F
C     INITIAL VALUES ARE SET UP. NOW GO THROUGH 8 ITERATIONS TO FIND
C     OPTIMUM B(I),F
    7 DO 95 L = 1,8
    8 DO 70 I = 1,3
      D(I) = 0.0
      BO(I) = B(I)
   10 B(I) = BO(I) + DLB(I)
C     KEEP B(I) WITHIN SPECIFIED RANGE
      IF(B(I)-A(I))15,12,12
   12 B(I) = A(I)
   15 CALL SHOOT(F,B)
```

```
      IF(F-FO)50,20,20
   20 B(I) = BO(I)-DLB(I)
C     KEEP B(I) WITHIN SPECIFIED RANGE
   21 IF(B(I)-C(I))22,22,25
   22 B(I) = C(I)
   25 CALL SHOOT(F,B)
      IF(F-FO)50,40,40
   40 B(I) = BO(I)
C     IF PROGRAM REACHES HERE THEN B(I) IS A LOCAL MINIMUM. IF THIS
C     HAPPENS FOR ALL B(I) THEN B(I) IS WITHIN ONE JUMP OF THE OPTIMUM
C     LET D(I)=1, RETAIN OLD VALUE OF FO (SKIP OVER FO=F)
      D(I) = 1.
      GO TO 70
   50 CONTINUE
C     WE HAVE A NEW VALUE OF B(I) AND F. NOW SEARCH IN ANOTHER DIRECTION
C     FROM THIS NEW POINT IN PARAMETER (B) SPACE
      FO = F
   70 CONTINUE
      SUMD = D(1) + D(2) + D(3)
C     WRITE PARAMETERS, ETC AFTER ALL PARAMETERS HAVE BEEN EXAMINED ONE
C     JUMP IN EACH DIRECTION
      WRITE(6,100)T,RHO,B(1),B(2),B(3),DELRMS,ACCEL,FO
  100 FORMAT(8F13.7)
C     IF ALL B(I) ARE WITHIN ONE JUMP OF OPTIMUM THEN REDUCE JUMP SIZE
      IF(SUMD-2.5)8,80,80
   80 DO 90 K=1,3
   90 DLB(K) = 0.1*DLB(K)
   95 CONTINUE
      GO TO 3
      END


      SUBROUTINE SHOOT(F,B)
C     ACCEL = RMS ACCELERATION/SQRT(2*PI*AV)
C     DELRMS = DELTA RMS/SQRT(2*PI*AV)
C     B(1)=ASUB1, B(2)=W(NATL FREQ), B(3)=Z(DAMPING RATIO)
      DIMENSION B(3)
      COMMON DELRMS,ACCEL,RHO,T
      S = SQRT(1. - B(3)**2)
      ACCEL=SQRT((B(2)**3*(B(1)**2 + ((1.-B(1))**2) + 2.*B(1)*(1.-B(1))*
     1(EXP(-B(3)*B(2)*T))*
     2(COS(S*B(2)*T) - (B(3)/S)*SIN(S*B(2)*T))))/(4.*B(3)))
      DELRMS =SQRT(((1. - 2.*(B(1) - 2.*(B(3)**2)) - 2.*(B(1)**2)*(4.*(B
     1(3)**2)- 1.)  + 2.*B(1)*(1. - B(1) + 4.*(B(3)**2)*(1. + B(1)))*(EX
     2P(-B(3)*B(2)*T))*COS(S*B(2)*T)+ 2.*B(1)*B(3)*(-1.+4.*(B(3)**2)*(1.
     3+ B(1)) - 3.*B(1))*(EXP(-B(3)*B(2)*T))*(SIN(S*B(2)*T))/S)/(4.*B(3)
     4*B(2))) - 2.*B(1)*B(3)/B(2) + (B(1)**2)*T)
      F = RHO*ACCEL + DELRMS
      RETURN
      END
```

APPENDIX B

EVALUATION OF INTEGRAL

$$\text{Evaluation of } I = \frac{1}{2\pi j}\int_{-j\infty}^{j\infty} \frac{\phi^n e^{\phi\sqrt{2}\,x}}{(\phi^4+1)^2}\, d\phi$$

When the denominator of above equation for I is factored, I may be written as

$$I = \frac{1}{2\pi j}\int_{-j\infty}^{j\infty} \frac{\phi^n e^{\phi\sqrt{2}\,x}}{(\phi+\frac{1+j}{\sqrt{2}})^2(\phi+\frac{1-j}{\sqrt{2}})^2(\phi-\frac{1+j}{\sqrt{2}})^2(\phi-\frac{1-j}{\sqrt{2}})^2}\, d\phi \qquad (B.1)$$

The integration indicated by Equation (B.1) is carried out by evaluating the residues of the four poles that lie in the contour taken around the left half plane. Thus

$$\text{Res}[(-1+j)/\sqrt{2}] = \frac{d}{d\phi}\left[\frac{\phi^n e^{\phi\sqrt{2}\,x}}{(\phi+\frac{1+j}{\sqrt{2}})(\phi^2-\sqrt{2}\,\phi+1)^2}\right]_{\phi=\frac{-1+j}{\sqrt{2}}} \qquad (B.2)$$

When Equation (B.2) is evaluated, we find

$$\text{Res}[(-1+j)/\sqrt{2}] = \frac{1}{16}\left(\frac{-1+j}{\sqrt{2}}\right)^{n-1} e^{(-1+j)x}\,[x-j(n-x-3)] \qquad (B.3)$$

Similarly

$$\text{Res}[(-1-j)/\sqrt{2}] = \frac{1}{16}\left(\frac{-1-j}{\sqrt{2}}\right)^{n-1} e^{(-1-j)x}\,[x+j(n-x-3)] \qquad (B.4)$$

Since $I = \text{Res}\,[(-1+j)/\sqrt{2}] + \text{Res}\,[(-1-j)/\sqrt{2}]$, Equations (B.3) and (B.4) may be combined to give a general expression for I as

$$I = \frac{1}{16} e^{-x} [A \cos x + B \sin x] \qquad (B.5)$$

where the coefficients A and B are given in the following table for values of n from 0 through 8.

n	A	B
0	$3\sqrt{2}$	$-\sqrt{2}(3+2x)$
1	$2x$	$-2(2+x)$
2	$-\sqrt{2}(1-2x)$	$\sqrt{2}$
3	$2x$	$2x$
4	$\sqrt{2}$	$\sqrt{2}(1-2x)$
5	$-2x$	$-2(2-x)$
6	$-\sqrt{2}(3-2x)$	$3\sqrt{2}$
7	$2(4-x)$	$-2x$
8	$-5\sqrt{2}$	$-5\sqrt{2}$

APPENDIX C

ANALOGY BETWEEN DETERMINISTIC AND RANDOM PROCESSES

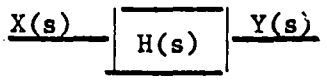

$$Y(s) = H(s)X(s)$$

Deterministic	Random
Parsevals theorem: $\int_{-\infty}^{\infty} y^2(t)dt = \frac{1}{2\pi j}\int_{-j\infty}^{j\infty} Y(s)Y(-s)ds$	The mean squared value of y may be given by $\frac{\overline{y^2}}{2\pi} = \frac{1}{2\pi j}\int_{-j\infty}^{j\infty} H(s)H(-s)\Phi_{xx}(s)ds$
For the above system $\int_{-\infty}^{\infty} y^2(t)dt = \frac{1}{2\pi j}\int_{-j\infty}^{j\infty} H(s)H(-s)X(s)X(-s)ds$	
For $X(s) = a/s$	For $\Phi_{xx}(s) = -AV/s^2$
$\frac{1}{a^2}\int_{-\infty}^{\infty} y^2(t)dt = \frac{1}{2\pi j}\int_{-j\infty}^{j\infty} \frac{H(s)}{s}\frac{H(-s)}{-s}ds$	$\frac{\overline{y^2}}{2\pi AV} = \frac{1}{2\pi j}\int_{-j\infty}^{j\infty} \frac{H(s)}{s}\frac{H(-s)}{-s}ds$

Therefore

$$\frac{1}{a^2}\int_{-\infty}^{\infty} y^2(t)dt = \frac{\overline{y^2}}{2\pi AV}$$

APPENDIX D

EVALUATION OF INTEGRAL

$$\text{Evaluation of } I = \lim_{\varepsilon \to 0} \int_{-j\infty}^{j\infty} \frac{\phi^n e^{\phi x}}{(\phi+\varepsilon)(\phi^2+2\zeta\phi+1)(-\phi+\varepsilon)(\phi^2+2\zeta\phi+1)}\, d\phi$$

The above integral may be evaluated by summing the residues of the three poles that lie within a contour taken around the left half plane. Thus

$$I = \text{Res } (-\varepsilon) + \text{Res } (-\zeta+j\sqrt{1-\zeta^2}) + \text{Res } (-\zeta-j\sqrt{1-\zeta^2}) \tag{D.1}$$

The residue at $-\varepsilon$ is given by

$$\text{Res } (-\varepsilon) = \frac{(-\varepsilon)^n e^{-\varepsilon x}}{2\varepsilon} \tag{D.2}$$

In the expression for $\delta_{p,rms}$ (Equation (76)) the numerator of one of the terms is of the form $1 - e^{\phi x}$. For this case

$$\text{Res}(-\varepsilon)_{1-e^{\phi x}} = \frac{1}{2} x \tag{D.3}$$

The residues at the poles $\phi = -\zeta \pm j\sqrt{1-\zeta^2}$ are

$$\text{Res}(-\zeta+j\sqrt{1-\zeta^2}) = \frac{(-\zeta+j\sqrt{1-\zeta^2})^{n-2} e^{(-\zeta+j\sqrt{1-\zeta^2}\, x)}}{8\zeta[1-\zeta^2+j\zeta\sqrt{1-\zeta^2}\,]} \tag{D.4}$$

$$\text{Res}(-\zeta-j\sqrt{1-\zeta^2}) = \frac{(-\zeta-j\sqrt{1-\zeta^2})^{n-2} e^{(-\zeta-j\sqrt{1-\zeta^2}\, x)}}{8\zeta[1-\zeta^2-j\zeta\sqrt{1-\zeta^2}\,]} \tag{D.5}$$

Thus I may be given in the following general form where the coefficients A, B, and C are listed below for several values of n:

$$I = \frac{e^{-\zeta x}}{4\zeta(1-\zeta^2)} [A \cos \sqrt{1-\zeta^2} + B \sin \sqrt{1-\zeta^2}\, x] + C \tag{D.6}$$

n	A	B	C
0	$(4\zeta^2-1)(1-\zeta^2)$	$-\zeta\sqrt{1-\zeta^2}(3-4\zeta^2)$	See Equation (D.3)
1	$-2\zeta(1-\zeta^2)$	$\sqrt{1-\zeta^2}(1-2\zeta^2)$	- 1/2
2	$(1-\zeta^2)$	$\zeta\sqrt{1-\zeta^2}$	0
4	$-(1-\zeta^2)$	$\zeta\sqrt{1-\zeta^2}$	0

REFERENCES

1. Paul, I.L., Bender, E.K., "Partial Bibliography on Subjects Related to Active Vibration Isolation and Active Vehicle Suspensions," Engineering Projects Laboratory, M.I.T., DSR 76109-2, November, 1966, PB 173 649.

2. Paul. I.L., Bender, E.K., "Active Vibration Isolation and Active Vehicle Suspension," Engineering Projects Laboratory, M.I.T., DSR 76109-1, November, 1966, PB 173648.

3. Bender, E.K., "Optimization of the Random Vibration Characteristics of Vehicle Suspensions," Sc.D. Thesis, Mechanical Engineering Dept., M.I.T., June 1967.

4. Bender, E.K., Karnopp, D.C., Paul, I.L., "On the Optimization of Vehicle Suspensions Using Random Process Theory," ASME Paper No. 67-TRAN-12.

5. Paul, I.L., "Design and Computer Simulation of a Near-Optimum Active Suspension System for High-Speed Ground Vehicles," 38th Shock and Vibration Symposium, St. LOuis, Mo., May 1, 1968.

6. Paul, I. L., Fenoglio, B.F., "Preliminary Design and Simulation of a Hydraulic Active Suspension System for High Speed Ground Vehicles," Engineering Projects Laboratory, M.I.T., DSR 76109-7, January 1968.

7. Wiener, N., "Extrapolation, Interpolation, and Smoothing of Stationary Time Series," Technology Press, Cambridge, Mass. 1949.

8. Newton, G.C.., Gould, L.A., and Kaiser, J.F., "Analytical Design of Linear Feedback Controls," John Wiley & Sons, New York, 1961.

9. Den Hartog, J.P., "Advanced Strength of Materials," McGraw-Hill, New York, 1952.

10. Edwards, L.K., "High Speed Tube Transportation," Scientific American, Vol. 213, No. 2, August 1965, pp. 30-40.

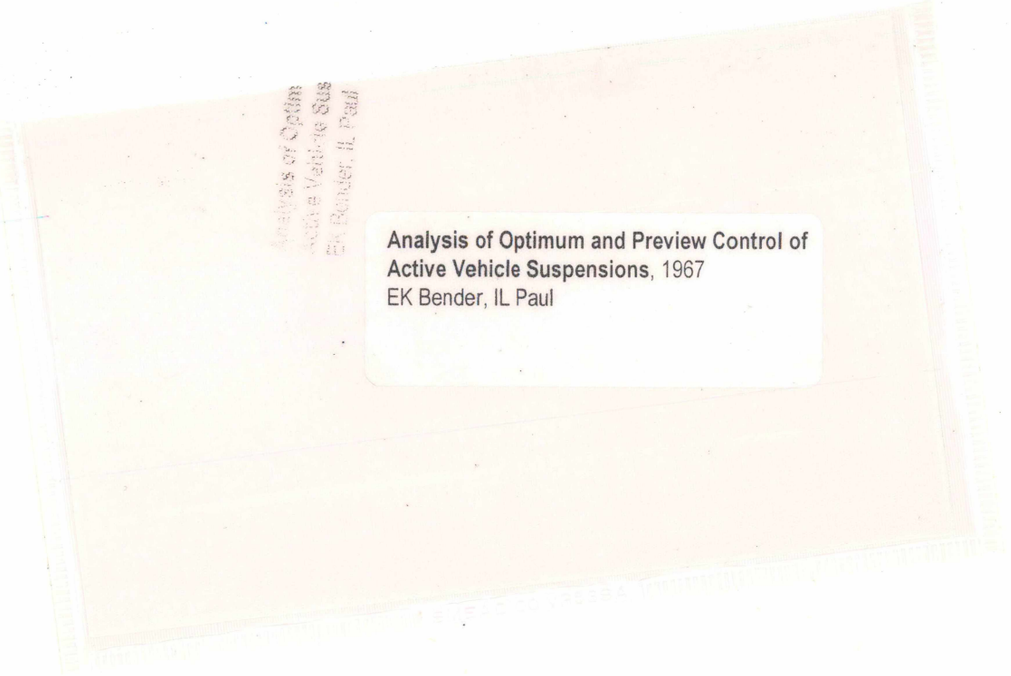

Analysis of Optimum and Preview Control of Active Vehicle Suspensions, 1967
EK Bender, IL Paul